File Cy:

AD A011254

ER-ES

BRL

REPORT NO. 1791

THE STRUCTURE OF THREE-DIMENSIONAL
SEPARATED FLOWS IN OBSTACLE-BOUNDARY
LAYER INTERACTIONS

Raymond Sedney
Clarence W. Kitchens, Jr.

June 1975

USA BALLISTIC RESEARCH LABORATORIES
ABERDEEN PROVING GROUND, MARYLAND

REPORT DOCUMENTATION PAGE		READ INSTRUCTIONS BEFORE COMPLETING FORM
1. REPORT NUMBER REPORT NO. 1791	2. GOVT ACCESSION NO.	3. RECIPIENT'S CATALOG NUMBER
4. TITLE (and Subtitle) The Structure of Three-Dimensional Separated Flows in Obstacle-Boundary Layer Interactions		5. TYPE OF REPORT & PERIOD COVERED Final
		6. PERFORMING ORG. REPORT NUMBER
7. AUTHOR(s) Raymond Sedney Clarence W. Kitchens, Jr.		8. CONTRACT OR GRANT NUMBER(s) RDT&E 1T161101A91A
9. PERFORMING ORGANIZATION NAME AND ADDRESS USA Ballistic Research Laboratories Aberdeen Proving Ground, Maryland 21005		10. PROGRAM ELEMENT, PROJECT, TASK AREA & WORK UNIT NUMBERS
11. CONTROLLING OFFICE NAME AND ADDRESS US Army Materiel Command 5001 Eisenhower Avenue Alexandria, VA 22333		12. REPORT DATE JUNE 1975
		13. NUMBER OF PAGES 59
14. MONITORING AGENCY NAME & ADDRESS(if different from Controlling Office)		15. SECURITY CLASS. (of this report) UNCLASSIFIED
		15a. DECLASSIFICATION/DOWNGRADING SCHEDULE
16. DISTRIBUTION STATEMENT (of this Report) Approved for public release; distribution unlimited.		
17. DISTRIBUTION STATEMENT (of the abstract entered in Block 20, if different from Report)		
18. SUPPLEMENTARY NOTES		

19. KEY WORDS (Continue on reverse side if necessary and identify by block number)

Vortex	Obstacles	Fluid Dynamics
Protuberances	Vapor Screen	Turbulent Boundary Layer
Attachment	Optical-Surface Indicator	Flow Structure
Three-Dimensional Separation	Flow Visualization	Primary Separation

20. ABSTRACT (Continue on reverse side if necessary and identify by block number) (jpl)

The subject is investigated with flow visualization techniques; the turbulent boundary layer on the wall of a continuous supersonic wind tunnel is used. Sizeable separated flow regions can be studied since the wall width is 38cm and the boundary layer is typically 2.5cm thick. The large scale of the experiment is required to resolve the fine details of the flow structure. The flow visualization techniques are discussed. The variation of primary separation distance is presented as a function of Mach number, Reynolds number, R, and
continued

20. Abstract (continued)

obstacle dimensions. Some scaling laws that have been proposed are not sup-
ported by our results. The structure of the separated flow upstream of the
obstacle changes with relatively small changes in R; the number of vortices
varies from 6 to 4 to 2 as R changes. Data are presented for large and small
protuberances, but the latter are emphasized.

TABLE OF CONTENTS

LIST OF ILLUSTRATIONS

Page

5

LIST OF ILLUSTRATIONS (continued)

6

LIST OF ILLUSTRATIONS (continued)

I. INTRODUCTION

Although the history of the study of boundary-layer or shear flows over obstacles is a long one, the recorded history extending back to Leonardo da Vinci, several aspects of such flows remain elusive. The main qualitative feature, the horseshoe vortex system, is well documented. The twin tornado-like vortices that rise up from the near wake and become the trailing vortex system have been studied for small obstacles. The third universal feature of the flow is the downstream persistence of these two vortex systems. A survey of the effects of small protuberances on boundary-layer flows[1] shows that the above three features are common to a wide range of conditions: laminar and turbulent boundary layers for all speeds up to hypersonic. However, more detailed examination of the flow structure is lacking except for laminar, low speed flow. One purpose of the present paper is to describe the flow structure for turbulent, supersonic boundary-layer flows over protuberances. Most of our experiments concern small obstacles; i.e., $k < \delta$, where k is the obstacle height and δ is the 99% boundary-layer thickness. However, data for large and intermediate obstacles are shown and their relationships with small obstacle data are discussed.

Since the flow structure, mainly the number and positions of vortices, is complex, the paucity of information on it is not surprising. The flow structure is needed not only to achieve an intuitive understanding of the flow but also to understand the pressure, heat transfer and shear distributions near and on the protuberance. These distributions and this understanding are needed for the well known applications in aerodynamics, ballistics and hydraulics; there are also applications in meteorology and geology. Recently, some features of the flow structure were used to interpret erosion patterns on Mars[2]. Data on pressure and/or heat transfer are available in many references, mostly for large protuberances. These are discussed in either Reference 1, the survey by Korkegi[3], or the report of Kaufman et al[4]. The very high values of pressure, pressure

1. R. Sedney, "A Survey of the Effects of Small Protuberances on Boundary Layer Flows," AIAA Journal, Vol. 11, No. 6, June 1973, pp. 782-792.

2. R. Greeley, J. D. Iversen, J. B. Pollack, N. Udovich and B. White, "Wind Tunnel Studies of Martian Aeolian Processes," Proc. Roy. Soc. Lond. A., Vol. 341, No. 1626, 10 December 1974, pp. 331-360. See also "Wind Tunnel Simulations of Light and Dark Streaks on Mars," Science, Vol. 183, March 1974, pp. 847-849.

3. R. H. Korkegi, "Survey of Viscous Interaction Associated with High Mach Number Flight," AIAA Journal, Vol. 9, No. 5, May 1971, pp. 771-784.

4. L. G. Kaufman II, R. H. Korkegi and L. C. Morton, "Shock Impingement Caused by Boundary-Layer Separation Ahead of Blunt Fins," AIAA Journal, Vol. 11, No. 10, October 1973, pp. 1363-1364. See also ARL 72-0118, Aerospace Research Laboratories, August 1972.

gradient, and heat transfer measured on and in the vicinity of large protuberances in supersonic flow are a most remarkable aspect of this separated flow. Such very high values are not found in the relatively few experiments on small protuberances. An unusual, and practically important, feature of this case is the fact that the disturbance caused by the small protuberance can persist for hundreds of protuberance heights downstream[1].

Understanding the flow structure and correlating the vast amount of data available is made difficult by the number of parameters that must be considered. The dimensions (three lengths), shape and orientation (sweep) of the obstacle are important. The undisturbed velocity profiles (laminar or turbulent, 2-D or 3-D) and δ must be considered as well as Mach number, M, and the Reynolds numbers that can be formed with the various lengths. The undisturbed velocity, U_k, at the height k off the surface has been found important in low speed flows. Heat and mass transfer and turbulent shear should be considered; we are unaware of any experiments which systematically vary these. This plethora of parameters is relieved somewhat for large protuberances; if $k \gtrsim \delta$ and the width is small compared to δ, then the height no longer influences the flow interactions, but the number of parameters is still large and unwieldy. Therefore, any success at correlating important flow features with the various non-dimensional combinations of parameters is important.

Such a correlation was given by Westkaemper[5] using a large collection of data on primary separation distance, S. This is defined as the distance from the leading edge of the obstacle to the most upstream location of separation. However, different definitions of separation were used in the data he collected. All the large protuberances were cylinders of diameter D, with $k > \delta$; the boundary layer was supersonic and turbulent. His conclusions were: $S/D = 2.65$ for $k/D > 1.13$ and $S/D = 2.42 \, (k/D)^{0.7}$ for $k/D < 1.13$; he proposes this correlation for $2 \leqslant M \leqslant 20$ and for all Reynolds numbers provided the boundary layer is turbulent. A critique of this is given later. Unfortunately, as more data become available, the deviation of the data from this correlation increases. However, this work indicates that S/D is essentially independent of Reynolds number; the variation with M is significant. Thus for large cylindrical protuberances the possibilities for correlation are favorable but less so for small protuberances, even if restricted to cylinders. Our data show that for constant Mach and Reynolds numbers, S does not scale with D. The number of models tested is not sufficient for us to arrive at definitive correlations.

The main objective of this work is to determine as much as possible of the flow structure. For this purpose flow visualization was used.

---

5. J. C. Westkaemper, "Turbulent Boundary-Layer Separation Ahead of Cylinders," AIAA Journal, Vol. 6, No. 7, July 1968, pp. 1352-1355.

The optical-surface indicator technique[6,7] was employed to visualize the flow patterns on the surface over which the boundary layer flows. More conventional techniques were used on the surface of the protuberance. The optical-surface indicator technique is particularly suited to this application and yields a vast amount of detail. For visualization off the surface, the vapor screen method was used since it is the only tracer method that will work in supersonic, turbulent flows. Although it provided some useful data, it is not as useful as the smoke method, which can provide many details in low speed, laminar flows. It could not, for example, resolve the multiple-vortex pattern upstream of the obstacles revealed by the optical-surface indicator visualization.

For a given protuberance and M we find 2, 4, or 6 vortices between the protuberance and primary separation, depending on Reynolds number. On physical grounds there is no reason why several vortices cannot exist there, but in the experiments on turbulent boundary layer - obstacle interactions, at either high or low speeds, two are almost always observed. An exception is the work of Winkelman[8]; he used a surface-indicator method in a high speed, turbulent boundary layer. The interpretation of our surface flow patterns was aided by the results of Norman[9], who used the smoke technique in a low speed, laminar boundary layer and obtained remarkably detailed information on the streamlines and vortices in the separated region. The structure in the separated flow upstream of the obstacle is fairly clear now but there are some features that must be clarified. The sensitivity of the number of vortices to changes in unit Reynolds number, R/ℓ, is an interesting fact for which we have no explanation at present.

Although we concentrate here on the upstream separated flow, many other features are revealed in our visualizations. Further work is required to gain sufficient insight into, e.g., the fascinating near wake

6. R. Sedney, "Visualization of Boundary Layer Flow Patterns Around Protuberances Using an Optical-Surface Indicator Technique," *The Physics of Fluids*, Vol. 15, No. 12, December 1972, pp. 2439-2441.

7. R. Sedney, C. W. Kitchens, Jr., and C. C. Bush, "The Marriage of Optical, Tracer, and Surface Indicator Techniques in Flow Visualization - A Survey," Record of the 1973 International Congress on Instrumentation in Aerospace Simulation Facilities, IEEE Publication No. 73CHO 784-9AES, pp. 155-171.

8. A. E. Winkelmann, "Flow Visualization Studies of a Fin Protuberance Partially Immersed in a Turbulent Boundary Layer at Mach 5," NOLTR 70-93, Naval Ordnance Laboratory, May 1970.

9. "R. S. Norman, "On Obstacle Generated Secondary Flows in Laminar Boundary Layers and Transition to Turbulence," Ph.D. Thesis, Illinois Institute of Technology, December 1972.

flow. Obtaining this insight and making progress on the items discussed at the end of the previous paragraph would be much easier if a model of this complex flow existed. On the other hand, the model can only be formulated after sufficient flow visualization is accomplished. This report represents one stage in this iteration process.

II. FLOW VISUALIZATION TECHNIQUES

In our experiments we visualize the flow in the following ways: (1) the optical-surface indicator method giving plan-view shadowgraphs that show surface flow patterns and shock fronts; (2) the conventional surface indicator method providing the flow pattern on the protuberance; (3) conventional, side-view shadowgraph and schlieren methods showing the trace of the shock surfaces and an indication of the edge of the boundary layer; (4) the vapor screen method giving shock surfaces, a boundary-layer edge and, to some extent, vortices. Because of the con- straints of the wind tunnel facility and for reasons of time and economy, we could not fully exploit all of these techniques. Most of our data was obtained with (1), considerably less with (3) and (4), and the least with (2). A more effective tracer method than the vapor screen technique is needed.

The tests were conducted in a continuous, supersonic wind tunnel, Supersonic Wind Tunnel No. 1 at the Ballistic Research Laboratories. The interactions were studied by placing the protuberances in the wall bound- ary layer, having a typical thickness of 2.5 cm. at M = 2.50. The optical-surface indicator method requires mounting the obstacle on a tunnel window which is in the sidewall. Obtaining the side-view shadow- graph and schlieren pictures requires placing the obstacle on the floor (or ceiling) of the tunnel. Pitot pressure surveys were made with no protuberance in the flow to determine the properties of and compare the floor and sidewall boundary layers. The data were taken at the point where the center of the protuberance would be. Figure 1 shows one set of the results; a separate report will contain all of them. The 99% velocity thickness, δ, is given as a function of unit Reynolds number, R/ℓ, and Mach number, M, for the sidewall and floor boundary layers. The only significant difference between these occurs at M = 3.50 for the low- est value of R/ℓ. We suspect the same trend exists at M = 4.50 but the results at small R/ℓ are not available for the sidewall boundary layer. Similar comparative results and trends are shown for displacement and momentum thickness. Thus for most test conditions a valid quantitative comparison can be made between results for the protuberance in the two locations.

The optical-surface indicator method will be described briefly; for more details see References 6 and 7. The obstacle is mounted on a test section window which is in a vertical plane. Figure 2 shows a schematic view of the experimental set-up and a sketch of some features of the flow over a small protuberance. A small amount of lightweight,

transparent oil is placed on the window before and/or after the flow is started. After the surface flow pattern is established, typically in one minute, a shadowgraph or schlieren picture is taken; we refer to these as plan-view pictures. They show the surface (window) flow pattern and parts of the shock surfaces. An example is shown in Figure 3. The relation between the streaks and flow near the surface is discussed in Reference 10.

The window used for these tests is one that has several pits and scratches from long use but is otherwise a "schlieren quality" window. The window defects are evident on the shadowgraphs. The model is bolted to the window. Schlieren pictures are taken by flashing a BH-6 tube. The schlieren light source and one parabolic mirror are used for contin- uous viewing on a frosty mylar screen. Shadowgraphs are taken with a spark light source of 1 μs duration.

Several methods of introducing oil onto the window are used. In the first method a light machine oil is sprayed on the window in a fine mist, usually upstream of the region where the primary separation of the boundary layer occurs. A second technique is to place regularly spaced dots on the window, usually near the model. A third method of introduc- ing oil makes use of a static pressure tap located 40 cm upstream of the model. Two or more drops of light machine oil are aspirated into the tunnel wall boundary layer. Some of the oil flows along the wall and window and some atomizes into the flow off the wall. The mist formed in this manner is carried in the flow to the region immediately upstream of the protuberance. Some impinges on the window, thus drawing the surface streamlines, and some is deposited on the protuberance. This is the only way that an attachment line, labeled A below, can be consistently visualized.

The clearest definition of the surface flow pattern is obtained when the oil drops are drawn out into streaks of height 0.1 mm or less. The intensity of the image of the streak is then about 50% of the undis- turbed intensity; it appears gray. If the cross-section of the streak is such that it is almost opaque, the spacing must be considerably greater to obtain a clear pattern, which decreases the resolution. The observed variation in intensity can be predicted approximately by geo- metrical optics calculations[7].

In Figure 3 most of the streaks are gray. Several prominent fea- tures are labeled. The attachment line A is difficult to see in a reproduction unless the region is enlarged, see References 1 and 7 for examples of that. If oil is placed near and upstream of the model before flow is started, it is mostly wiped away by the time a shadowgraph

---

10. R. L. Maltby, "Flow Visualization in Wind Tunnels Using Indicators," AGARD-ograph 70, AGARD-NATO Fluid Dynamics Panel, 1962.

is taken. If oil is introduced through the pressure tap, a clear image
of A is obtained for a few minutes. This is the region of highest shear
and, from the results of other investigators, e.g., Reference 8, highest
heat transfer. As in all shadowgraphs, a shock wave surface will pro-
duce a shadow only if there are light rays at nearly grazing incidence
to the surface. Since the cylinder in Figure 3 is a large protuberance,
the shock pattern is not like the side view sketched in Figure 2. It
consists of a bow shock which intersects a separation shock, well below
the top of the cylinder, resulting in a Mach stem plus other complex
structure. A visualization of this will be shown in Figure 5. For the
conditions of Figure 3, the bow shock is steady and hence has a distinct
shadow; the Mach stem is unsteady which explains its irregular shadow.
This unsteadiness is shown in our side-view shadowgraphs and has been
found by other investigators. The dominant frequency of the oscillation,
from other kinds of shock intersection studies, is probably on the order
of 1000 Hz. The shear at the wall, which forms the surface flow pattern,
has a dominant frequency which is presumed to be much less. At any rate
a surface indicator method can only give an indication of an average
flow pattern.

The usual surface indicator method of coating the model with a pig-
mented oil was used to observe the flow pattern on the protuberance. A
variation of this, which incorporates the idea of taking a shadowgraph
of transparent oil streaks, was also used. The model was wrapped with a
transparent plastic sheet and oil was introduced through the upstream
pressure tap with flow in the tunnel, as explained above. At the end of
the run the wrapping was removed and a shadowgraph of it was taken.
Obviously this method is only convenient if the surface of the protuber-
ance is developable. Surface flow patterns on the front half of a large
and a small cylindrical protuberance are shown in Figure 4. Somewhat
different patterns are obtained for a large cylindrical protuberance
depending on k/δ, D/δ, M, and R/ℓ, see References 8 and 11. The pattern
shown in Figure 4a is like that of Reference 11 except for the upper por-
tion. In that reference k/δ was large enough so that the circumferential,
2-D flow, was approached. We are unaware of other work that shows the
surface flow patterns on a small protuberance. A distinguishing feature
of the pattern shown in Figure 4b is the attachment point on the central
generator at the top of the cylinder. There is an intimate relation
between the separation line near the bottom of each cylinder and the
attachment line A mentioned above; this will be discussed later.

The side-view shadowgraph and schlieren visualizations will not be
discussed except to mention that a sampling of the unsteady behavior of

11. D. M. Voitenko, A. I. Zubkov and Y. A. Panov, "Existence of Super-
     sonic Zones in Three-Dimensional Separation Flows," Izv. AN SSSR.
     Mekhanika Zhidkosti i Gaza, Vol. 2, No. 1, 1967, pp. 20-24.

the Mach stem and some weak waves from the separated shear layer was obtained by taking a sequence of shadowgraphs using the 1 μs light source.

The vapor screen method is the only tracer method available for the flow under consideration, leaving aside the use of tufts. It is described fully by McGregor in Reference 10. Our version of the method is different from the standard practice only in the way the light sheet is generated. This is done in a simple fashion[12] using a low power CW laser (e.g., 15mW), a cylindrical lens (a glass rod is adequate), and a small slit to cut off some undesirable side bands of light. Some further details of this are given in Reference 7. The small diameter beam is diverged by the lens into a light sheet of thickness equal to the beam diameter. The sheet is rotated by rotating the lens and is easily translated because the apparatus weighs little.

In the vapor screen method one observes the light scattered by the liquid or solid particles which are usually water. Shock waves and vortices are easily detected. An example is shown in Figure 5 for flow over a large cylindrical protuberance. In this example the light sheet is in the plane of symmetry of the flow, the horizontal plane, which contains the axis of the cylinder. It is observed through the vertical window and photographed with a camera at 30° to the sheet. The perspective of this oblique side view makes interpretation of these visualizations more troublesome than true side views (90° to sheet). The illumination is determined by the density of scattering centers and this is changed by mechanical and thermodynamic effects. Near the window heat transfer effects also enter. These heat transfer effects, together with the fact that some of the vortices we wish to see are small and closely spaced, have prevented us from resolving some of the more interesting flow patterns. Finally, care must be taken if quantitative results are desired since the condensation process alters the flow properties.

III. MODELS AND TEST CONDITIONS

The test section of the wind tunnel is 33 x 38 cm in cross-section and the protuberances were mounted on the 38 cm wall. Data were taken at M = 1.5, 2.5, 3.5, 4.0, and 4.5, but mostly at M = 2.5 and 3.5. The unit Reynolds number was varied over the allowable limits which are shown by the values in Figure 1. The stagnation temperature is nominally 90°F. The experiments were performed using obstacles of simple geometrical shape: circular cylinder, hemisphere, parallelepiped, truncated cone, and bar. The last was used in a study of side plate design so that

---

12. *Private communication from R. K. Matthews, Arnold Engineering and Development Center, to C. J. Nietubicz, Ballistic Research Laboratories, 1972 and 1973.*

the flow over a projectile rotating band could be simulated; that work will be reported separately. For the first four obstacles we also added a small perturbation to the basic shape but space limitations preclude discussion of the results. For the same reason we give no details for the flow patterns about the hemisphere, parallelepiped, and truncated cone. Table 1 gives the dimensions of the models, the notation used in referring to them (e.g., 2C), and the symbols used when plotting results for several models on the same figure.

IV. PRIMARY SEPARATION

One of the quantities of primary interest in obstacle-boundary layer interaction is the extent of the separated flow, bounded by a curve called the primary separation line; it is required to estimate the loads on the surface. We define the distance from the leading edge of the obstacle to primary separation to be S, for obstacle-boundary layer flows with a flow symmetry plane. Westkaemper[5] discussed how a knowledge of S can be used, together with some empirical correlations, to estimate the position of the triple shock intersection and the maximum pressure on the leading edge. His estimate of pressure was 20% high in one case. Although the primary separation line is easily determined from our plan-view shadowgraphs it is only practical to discuss the behavior of S. Because we simultaneously visualize the bow shock, correlation of it with the primary separation line is straightforward. Our measured bow shock detachment distances for models 1D and 2D agree with those in the literature for 2-D flow over cylinders to within 5%.

A question arises as to how separation is defined from experimental measurements. In the kinds of flows considered here it has been defined using pressure or heat transfer distributions, side-view schlieren or shadowgraph photographs, and surface indicator techniques. The fact that these give different results has been discussed in the literature (especially for 2-D flows); we will not elaborate on this. Note that Price and Stallings[13] make a distinction between the disturbed flow region, as determined by pressure measurements for example, and the separated flow region, as determined by surface indicators. General use of such a convention would obviate confusion. Unsteady effects, which certainly exist in the flow, will affect the experimental definition of separation in different ways for the various measurement techniques. Suffice it to say that the surface indicator technique, with its extremely slow response time, gives an indication of an average surface flow pattern that is clear and repeatable. Unsteadiness in flows of the type considered here is discussed in Reference 4 with respect to static

13. E. A. Price and R. L. Stallings, "Investigation of Turbulent Separated Flows in the Vicinity of Fin-Type Protuberances at Supersonic Mach Numbers," NASA TN D-3804, February 1967.

pressure measurements; the conclusion is reached that the pressure distributions are not repeatable.

The accuracy of the measured values of S is, in most cases, ± 1%. At the lowest stagnation pressures at each Mach number this becomes ± 3%. These error bounds include effects from both repeatability of the pattern and reading accuracy. Additionally, there is a slight amount of geometrical magnification in the images on the shadowgraph because we use diverging light from the spark source. This systematic error is easily accounted for. Most often this correction is negligible, but in some cases it amounts to 5% in the ratio S/D.

The primary separation distance, for cylinders say, is a function of the following variables: D, k, δ, free stream velocity, U_k (for small protuberances), kinematic viscosity, sound velocity, density, and a measure of the turbulent shear. We have no measure of the turbulent shear and we find that U_k is not significant as an independent variable, so these are left out of the dimensional analysis. This yields

$$S/D = f(k/D, D/\delta, R_D, M);$$

where R_D is Reynolds number based on D and free stream velocity. Of course this can be written in other equivalent forms, so that, e.g., k/δ and R_k appear as two of the four non-dimensional parameters. It is often convenient to use the three ratios of lengths even though they are not independent. Likewise, three Reynolds numbers could be defined; we do not have enough points in parameter space to tell which of these is most meaningful. The variation of S/D with any of these Reynolds numbers is weak compared to the other three non-dimensional parameters.

Curves of S/D versus k/δ are given in Figure 6 to show the approach to an "infinite length" cylinder. For each of the curves three of the four possible dimensionless parameters are constant, viz., D/δ, R_D, and M. From the data in the literature, and as expected, S/D approaches a constant as k/δ increases. If a large protuberance is defined on that basis, then clearly models 1D and 2D, with k/δ = 4.5, are large. Other definitions are possible, e.g., requiring 2-D flow on some portion of the cylinder. On that basis these models are not large, see the cylinder surface flow sketched in Figure 4; a much larger k/δ would be needed. We shall adopt the definition based on S/D. The results in Figure 6 show that the rate of approach to the asymptote depends on D/δ.

The same kind of conclusions are reached if the data for M = 3.5 are plotted in the same way. Instead this data is presented in Figure 7 with the roles of k/δ and D/δ interchanged. Again, models 1D and 2D with k/δ = 3.69 are large protuberances; the variation of S/D with D/δ is only slightly larger than the estimated error in S/D. Thus these two data

points are consistent with the results of many other investigators, viz., that S/D is independent of D for a large cylindrical protuberance. Contrast this with the conclusion for the small protuberance, e.g., S/D changes by more than a factor of 2 for k/δ = 0.37. The simple and satisfying scaling law valid for large protuberances is not valid for small ones. The integers which appear above each data point refer to the number of vortices found between the obstacle and primary separation, as discussed in the next section.

Another conclusion reached in some other studies of separation caused by large, cylindrical obstacles is that S/D is weakly dependent on M. This dependence, for the large cylinders 1D and 2D, is shown in Figure 8. The variation in S/D is more than 50%; whether or not this is a weak dependence is a matter of interpretation since the term is not a precise one. The data points are connected with straight lines as a reading aid. For the small protuberances a variation of S/D with M is established only for model 2B; but the trend of increasing S/D with M is clear for all models. Note that, even though R/ℓ is constant, δ varies because M changes. Thus the change of S/D with M and k/D, shown in Figure 8, is affected by other parameters.

The next two figures give a partial evaluation of the correlation for large protuberances proposed by Westkaemper[5] and indicate the extent to which our data for small protuberances agree with it. In Figures 9 and 10 data for S/D versus k/D are shown together with the correlation of Reference 5, already discussed in the Introduction. Since R/ℓ and M are fixed in each case, δ is constant. Points for constant k/δ or D/δ can be connected with the help of Table 1. At M = 2.5 our two points for large k/δ are well below the correlation, as are the two from Reference 4 and the five points from Reference 14; the latter are for an "infinite effective height" but unspecified k/D. The data from these two references are for the same M but for a larger R/ℓ; they were determined using surface indicator methods. Our data for the small protuberances bear little relationship to the correlation, as might be expected; Westkaemper[5] cautions against using the correlation for cylinders "that do not extend to the outer edge of the boundary layer." From our previous discussion (Figure 6) the condition would be more restrictive than that. Thus at M = 2.5 the correlation is not very successful. The situation is a little better at M = 3.5. Our points are closer to the correlation but the two points from Reference 4 are not. The latter are for M = 3.0 and 4.0; the value of S/D for M = 3.0 is less than that for M = 2.5 in Reference 4 even though the values of k/D are not much different. Our data, for M = 1.5, 4.0, 4.5 are consistent with the trend shown in Figures 9 and 10. The data points for the large protuberances

14. D. M. Voitenko, A. I. Zubkov and Y. A. Panov, "Supersonic Gas Flow Past a Cylindrical Obstacle on a Plate," Mekhanika Zhidkosti i Gaza, Vol. 1, No. 1, 1966, pp. 121-125.

agree with the correlation for M = 4.0 and lie above it for M = 4.5. The data, from various sources, used in establishing the correlation extend over the range 2 < M < 20, but separation was determined in different ways in these sources. In several of these sources, separation was determined by noting the first change, in a pressure or heat transfer gauge reading, from the undisturbed, upstream reading. That method will give a separation distance larger than the surface indicator method. The latter was used by Westkaemper[5] to obtain his own data points that went into the correlation. The surface flow pattern was visualized in his experiments by injecting a liquid through an orifice upstream of primary separation. From a photograph of the pattern it is seen that a horseshoe vortex from the injection orifice interacts with primary separation; this has been noted by others, see Reference 7. This interaction will introduce an error in S of unknown amount. If the interference of the orifice vortex and wake flows with primary separation acts to increase S, then some unclear points about the correlation could be understood.

Regardless of the agreement of the data with this particular correlation, it is evident that the spread in the data for small protuberances is reduced most by plotting S/D versus k/D. One tentative possibility for correlation, including small and large cylinders, would be to consider S/D as a function of k/D for fixed M, but variable Reynolds number, e.g., by fairing a curve through the points of Figure 9. A wider range of the other parameters, D/δ, etc., is needed to arrive at a more firm conclusion. The result that S/D is almost independent of D but depends on M for large cylindrical protuberances is reasonable if the inviscid pressure field is considered. There is then only a bow shock, and its detachment distance, Δ, scales with D. The pressure change across this nearly 2-D shock is independent of D but depends on M. Thus the pressure gradient imposed on the boundary layer has the same dependence. For the small cylindrical protuberances, the inviscid flow bow shock position depends on k/D and M and the pressure change across it depends on M. Therefore, it is reasonable that, for this case, k/D and M have a significant affect on S/D. That is what our data show.

Variations of S/D with a Reynolds number will not be shown. To obtain a significant change in, say, R_D by changing D and also keeping the other dimensionless parameters approximately constant, would require many more models than we have used. Because of limitations of the wind tunnel and small changes in δ with R/ℓ, even a factor of two change in R_D would be difficult to achieve if, e.g., D/δ were held fixed. Therefore, changes in R/ℓ must be utilized. Examples of S/D versus R/ℓ are included in the figures discussed in the next section. For all of our models the conclusions are that: (1) for fixed D and k, S/D changes by 30% at most for the maximum allowable variation in R/ℓ, with most of that change taking place at the lower end of the range of R/ℓ; (2) S/D sometimes decreases while for other models it increases as R/ℓ increases; for several models S/D is a non-monotonic function of R/ℓ. This variety in

the behavior of S/D is related to the changes in the flow structure as R/ℓ is varied.

V. FLOW STRUCTURE

Detecting the magnitude and kinds of changes of S/D with R/ℓ just mentioned by means of pressure or heat transfer measurements on the surface would be extremely difficult and impossible using side-view shadowgraphs. With conventional surface indicator techniques it is more likely, but this has not been done. The optical-surface indicator technique can detect this behavior without much difficulty when used with a little care; it visualizes many other features of the flow, several of which are now discussed.

A. Upstream

For convenience we shall divide the flow into the regions upstream and downstream of the center of the cylinder. It is best to start the description of the upstream flow in and near the plane of symmetry. Separation and attachment lines have a special appearance in that plane. The 3-D vortices implied by these lines have helix-like streamlines and the pitch of the helix goes to zero as the symmetry plane is approached. Because of symmetry, there is no flow across this plane but there is flow out of or into it so that streamlines can appear to end in a side view of this plane, being tangent to it. We shall use the same symbol (e.g., S for primary separation) to represent a point in the plane of symmetry, its distance from the leading edge of the cylinder, and its continuation as separation or attachment lines. These lines show that there must be vortices off the surface and it is convenient to describe the flow structure in terms of the number of these vortices. The relationship between separation and attachment lines and the number of vortices will be clarified by referring ahead to Figure 17. There could be additional vortices further off the surface which leave no trace; the flow off the surface is discussed later.

An example of two vortices is shown in Figure 3; there is one separation point, S, and one attachment point, A, in the plane of symmetry. The two-vortex pattern is most often found in turbulent boundary layer-obstacle interactions. The streamwise extent of the large vortex is about 25 times that of the small one, as indicated by the surface pattern.

For a given small or large cylinder, at fixed M, the number of vortices changes with R/ℓ. Our results show as many as 6 of them. The separation and attachment lines for 6 are shown in Figure 11a; the change to 4 and then to 2 is sketched in Figures 11b and 11c. Note that S and A are always present, but the structure between them changes. A plan-view shadowgraph, obtained by the optical-surface indicator technique, is shown in Figure 12 to illustrate the 6 vortex pattern. The sequence in Figure 11a, b and c shows the number of vortices decreasing as R/ℓ

20

changes. These sketches are not to scale, but the sequence is that shown in Figure 13 as R/ℓ increases. We shall refer later to a 4-inner vortex configuration. This denotes the situation of 11b wherein A2 and S2 are not present. If A1 and S1 have disappeared, but A2 and S2 remain, this is called a 4-outer vortex configuration.

The distances from the cylinder leading edge to the points as shown in Figure 12, normalized by D, are shown in Figures 13, 14, and 15. The symbols are defined on Figure 14. The abscissa is the stagnation pressure, P_o, which, for fixed M, is proportional to R/ℓ; a value of R/ℓ is included to facilitate conversion from P_o. In particular the variation of S/D with R/ℓ, discussed in the last section, is given. The scatter in S/D for the low values of P_o, mentioned before, is also illustrated. The most difficult position to determine is A2. The main problem is to introduce the oil in such a way that there is some in the neighborhood of A2 after flow is established. If oil is aspirated into the tunnel, after flow is established, some will reach S2 but a clear pattern at A2 is not obtained. In Figures 13 - 15 straight lines connect the points or their average, for ease in following the trends. In addition, dashed lines are used to extend the trend. The paths followed by the various points will be described for Figure 13. At the lowest P_o there are 3 attachments and 3 separations, therefore 6 vortices as indicated at the top of Figure 13. Point A stays fixed; it is associated with S and is always present. The distance S decreases suddenly between 35 and 50 cm Hg and thereafter changes little. This decrease appears to be related to the disappearance of A2 and S2 which takes place for P_o between 35 and 40 cm Hg. Point A1 does not change much but S1 approaches it and then they disappear. This is the sequence of events depicted in Figure 11. The sequence is different in Figure 14, which shows the same type of data for the same small protuberance but for M = 3.50. For $P_o \leqslant 150$ the 4-inner vortex structure exists, but disappears for $P_o > 150$. The 4-outer vortex structure appears for some $P_o \leqslant 150$. For $P_o = 150$ we have 6 vortices. As P_o increases the number of vortices goes from 4 to 6, to 4, to 2. That such phenomena also take place for large protuberances is shown by Figure 15 which is for M = 3.50. The paths of the points are very much like those in Figure 14. There is no data in the small range of P_o between the 4-inner and 4-outer structures, so we cannot definitely say that 6 vortices exist. For the three cases illustrated and the others where we have enough data to draw conclusions, the relatively rapid decrease in S/D for a small increase in P_o is associated with the disappearance of A2 and S2.

The details of the process by which an attachment and a separation line merge and then disappear, in or near the symmetry plane, have been observed. From these visualizations the sketches shown in Figure 16

were drawn, for a 4-inner vortex structure. Parts a and b illustrate the motion of A1 and S1 towards each other. When they meet, part c, an unusual pattern is obtained; it is like one-half of the pattern that would be obtained at a nodal point of attachment juxtaposed with the separation line, see Reference 7 for an example. Upstream of S, the pattern is like that shown in Figure 4b. Finally, S1 bifurcates so that near the plane of symmetry the separation line has disappeared and there is flow through the center of S1. The two branches of S1 are still separation lines; they are similar to the open type separation lines that have been found in the flow over inclined bodies of revolution, see for example Reference 15.

We have not yet detected any regularity in these changes in flow structure. They occur for rather small variations in Reynolds number. This suggests there may be a delicate balance in the flow which is upset by changing R/ℓ so that one structure easily changes to another. Note that the results of Figures 13 - 15 are repeatable from test to test and can be obtained either by starting tunnel flow at a certain P_o or varying it continuously during a test. Therefore, it would not seem proper to call these changes an unstable behavior. Similar flow structure changes have been observed in low speed, laminar flow over small protuberances; e.g., in Reference 9. Norman states that "We have seen one, three, five, and even seven steady vortices forming in front of upright cylinders and fences of varying widths as k/δ and/or U_∞ increased." He observed the changes in the number of vortices to occur in "discrete jumps." The odd number of vortices observed by Norman is consistent with our even number. He did not observe the small vortex at the base of the protuberance, or the attachment point A; the size of this vortex makes it difficult to see using the smoke technique.

We shall now discuss the flow off the surface but still in the neighborhood of the plane of symmetry. This involves some conjecture since we mostly have surface data; the vapor screen technique could not resolve the multiple-vortex structure just discussed. Elementary fluid dynamic reasoning allows possible vortex structures to be determined. An attempt at this was made in Reference 6, with insufficient surface data to support the conjecture. We use the work of Norman[9] to aid our conjecturing and give it a more firm basis. His careful use of the smoke technique gave him some beautiful views of streamline patterns. Some of these are shown and discussed by Morkovin[16]. From the

---

15. E. C. Maskell, "Flow Separation in Three Dimensions," Rept. No. Aero 2565, Royal Aircraft Establishment, Farnborough, November 1955.

16. M. V. Morkovin, "An Approach to Flow Engineering via Functional Flow Modules," Beiträge zur Strömungsmechanik, insbesondere zur Grenzschichttheorie, Porz-Wahn, DLR F Vol. 2, pp. 270-301, 1972.

22

visualization in the neighborhood of the plane of symmetry, two possible models of the vortex structure were determined, called the "jet-maze" and "stairstep" models; the former was preferred. We have adapted and modified his rendition of the jet-maze model, with 6 vortices, in Figure 17a. The modifications are: (1) we have no attachment point on the protuberance, since the surface flow on small cylinders showed none, see Figure 4b; (2) we have separation near the base at point P for the same reason; (3) we have an attachment point, A, already discussed. The sketches are not to scale and the streamwise dimensions are magnified compared to cross-stream dimensions for clarity. For the same reason the shock surfaces are omitted. Figures 17b, c, and d show the 4-outer, 4-inner, and 2 vortex structures assuming the jet-maze model applies to all of them. The distances from the junction of the plane and cylinder to points A and S are approximately equal. But A and S cannot be connected by a streamline to have a closed vortex, by conservation of mass. The flow near A comes from high energy flow near the edge of the boundary layer, which is probably why the high shear exists there, as discussed before. In Winkelman's experiments[8], A is in the center of the highest heat transfer region on the surface. Norman[9] did see a smoke line following the tortuous path leading to A2 in 17a, which is not present in the stairstep model. In our experiments, when oil is introduced through the pressure tap, some is deposited near S1, A1, S2, and, to a lesser extent, near A2. Since we have no quantitative measure of the distribution of droplets through the boundary layer, this information does not allow a deduction in favor of either the jet-maze or stairstep model. To appreciate Figure 17 it is well to refer back to Figures 11 - 15. The delicate balance of the vortex structure, mentioned above, may be associated with the existence of the free stream stagnation points shown in Figure 17.

If we now briefly consider the flow away from the symmetry plane, the primary separation line, S, remains distinct over the field of view. But for some of the smaller models, for which more of the flow field is visible, this line becomes very hard to distinguish. The attachment at A continues as a fairly distinct attachment line to at least behind the model, see Figure 3. The other attachment lines, when they exist, become less distinct more quickly. This is also true for S2, but usually not for S1, which may mean that S2 lifts off the surface but S1 remains near it. A vapor screen photograph, with the light sheet perpendicular to the cylinder axis, clearly shows one horseshoe-shaped dark region indicating that the horseshoe vortex remains intact to at least 3 diameters downstream. Some painstaking work gave Norman a visualization of his flow around the side of the obstacle and some sketches of the vortex structure. These may help us to interpret our surface patterns.

B. Downstream

This part of the flow contains a number of fascinating features, some of which will be briefly discussed. More detail will be given in a separate paper. Outside the wake there is still at least one vortex,

23

meaning one leg of the horseshoe vortex. A secondary separation line
exists even if there is none immediately upstream of the model. From
other studies the horseshoe vortex is known to persist for hundreds of
protuberance heights downstream[1]. The near wake patterns of all of our
small protuberances listed in Table 1 are the same, topologically. This
statement requires that model 1C not be called small as it was in our
definition; actually, it is perilously close to being large, see Figure
6. A sketch of one of these patterns is shown in Figure 18. An attach-
ment line is shown as a dashed line. The attachment line that crosses
the plane of symmetry is almost certainly the impingement of the flow
that separates from the top and/or the sides of the protuberance. Flow
from this attachment line, in addition to other parts of the flow field
as shown, feed into the two large dots in a swirling manner. In the
shadowgraphs we see two oil accumulation dots, as in Figure 3; this shows
a large protuberance flow pattern but the phenomenon is the same. Suf-
fice it to say that these dots appear for all of our small-obstacle near
wake flows. They are the surface traces of the two tornado-like vortices
discovered by Gregory and Walker[17]; they rise up from the surface, bend
over into the free stream direction, and continue as the trailing vortex
pair. The small protuberance near wake surface pattern illustrates
Morkovin's base flow-through module[16] for high speed turbulent flow.
Some further discussion of this can be found in Reference 1. For differ-
ent orientations of the light sheet, the vapor screen shows only a dark
region in the new wake; apparently it cannot resolve this complex struc-
ture, at least not near a wall. When the sheet of light was placed nor-
mal to the surface (and free stream) at distances between 1.5 and 4.0
diameters downstream of the cylinder leading edge, contrasting light and
dark regions were observed. Specifically, a dark region of oval shape
is seen; the width to height ratio is typically 3.0, see Figure 19. The
long axis is parallel to the surface and the bottom is roughly (0.1) k
off the surface. The position of the two ends, along the major axis of
the oval, correlates with the attachment lines A_w in the oil flow sur-
face pattern, Figure 18. If the trailing vortices remained stable we
would expect to see two distinct, dark regions indicating their cross-
sections. We suppose there are two such regions which are not resolved.
The surface pattern, as seen in Figure 18, is consistent with the con-
jectured interpretation. If the direction of rotation observed in the
vortices normal to the surface (the dots) is continued downstream, as in
the trailing vortices, then the centerline of the wake would be a sepa-
ration line and there should be two, symmetrically located attachment
lines. This is what we observe, as in Figure 18, for all small protu-
berances. Since our shadowgraphs for all small protuberances show the
two dots and separation along the wake center line, we are fairly cer-
tain that the above conjecture is correct, at least in an average sense,
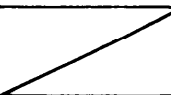
---

17. N. Gregory and W. S. Walker, "The Effect on Transition of Isolated
     Surface Excrescences in the Boundary Layer," R & M 2779, Pt. I,
     1955, Aeronautical Research Council, England.

for the first few diameters downstream. As the vapor screen is translated downstream the dark region changes shape and gradually rises off the surface. The changes in the near wake as R/ℓ is varied are minor. The effect of M is more noticeable, the change from M = 1.5 to 2.5 being greater than that from M = 2.5 to 4.5. These are not qualitative changes, as mentioned at the beginning of this subsection.

In contrast, for large protuberances there are qualitatively different near wake patterns as R/ℓ and M vary; compare the shadowgraph in Figure 3 with the sketch of the near wake presented in Figure 20. For instance the dot-swirl feature is shown in the former but not in the latter. Sometimes we see oil accumulation dots attached to the cylinder, fed in the manner shown in Figure 20. The dots are generally on the model for low values of R/ℓ and move downstream monotonically as R/ℓ increases, at a fixed M. (Figures 3 and 19 are for different values of M.) That no attachment line is observed, such as the one normal to the centerline in Figure 18, is understandable. One feature is common to all of our large protuberance cases, now including model 1C. That is, the centerline of the far wake is always an attachment line. Contrast this with the small protuberance finding. The far wake, as visualized by the vapor screen, is considerably more complex for large protuberances, compared to the small protuberance case. More analysis of our vapor screen results remains to be done. An example of one view of the wake, in a plane three diameters downstream of the leading edge of a large cylinder, is shown in Figure 21. Some of the intricate detail, at a distance k off the surface, is lost in the reproduction. Near the surface, instead of the dark region being oval-like, as for the small protuberance, it is shaped more like a triangle with curved sides and rounded vertices, with the bottom "side" parallel to the surface. To explain the flow pattern of Figure 19 there must be two vortices in the bottom part of the triangle, with circulation such as to produce the attachment line; i.e., opposite to that in the small protuberance case. Understanding such a 3-D wake requires more visualization of the flow structure.

Table 1. Model Dimensions (cm), Designation (e.g., 2C) and Plotting Symbols.

CYLINDERS

		A		B		C		D	
1	k D	1.02 1.91	◆	2.03 1.91	●	4.06 1.91	■	10.16 1.91	▲
2	k D	1.02 3.81	◊	2.03 3.81	◔	4.06 3.81	◰	10.16 3.81	△
3	k D	1.02 7.62	◇	2.03 7.62	○	4.06 7.62	□		
4	k D	1.91 HEMISPHERE 3.81							
5	k D	2.03 TRUNCATED CONE 3.81 (Base) 1.91 (Top)							
6	k	2.03 PARALLELEPIPED 2.54 (Width) 2.03 (Depth)							

Solid Symbol – Sidewall B.L.
Open Symbol – Floor B.L.

M = 4.5

Figure 1. Boundary-Layer Thickness (δ) vs. Unit Reynolds Number from Pitot Surveys.

27

LIGHT RAYS

M > I

SHOCKS
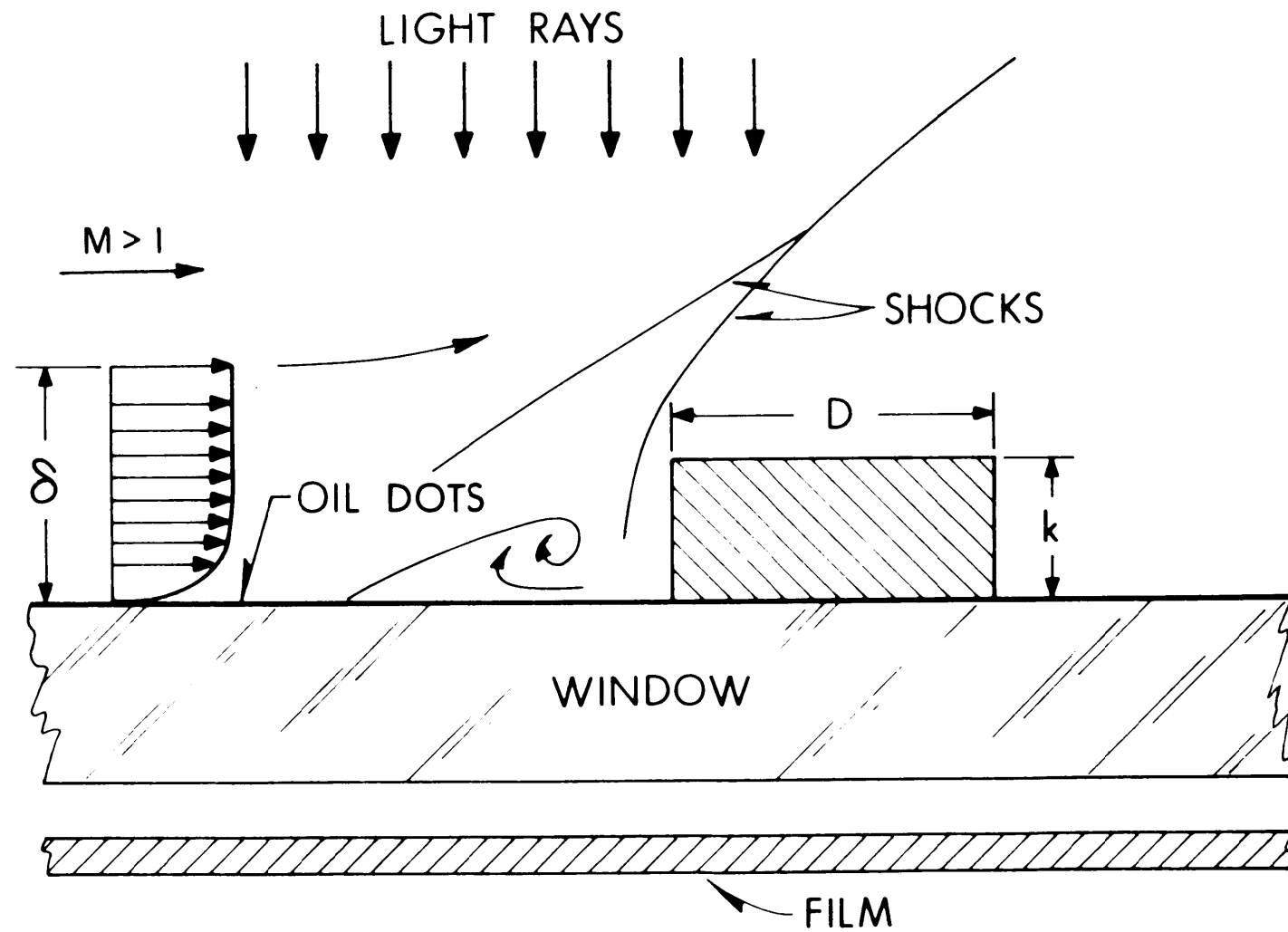
δ

OIL DOTS

D

k

WINDOW

FILM

Figure 2. Schematic of Optical-Surface Indicator Technique Showing Small Protuberance Immersed in Supersonic Turbulent Boundary Layer.

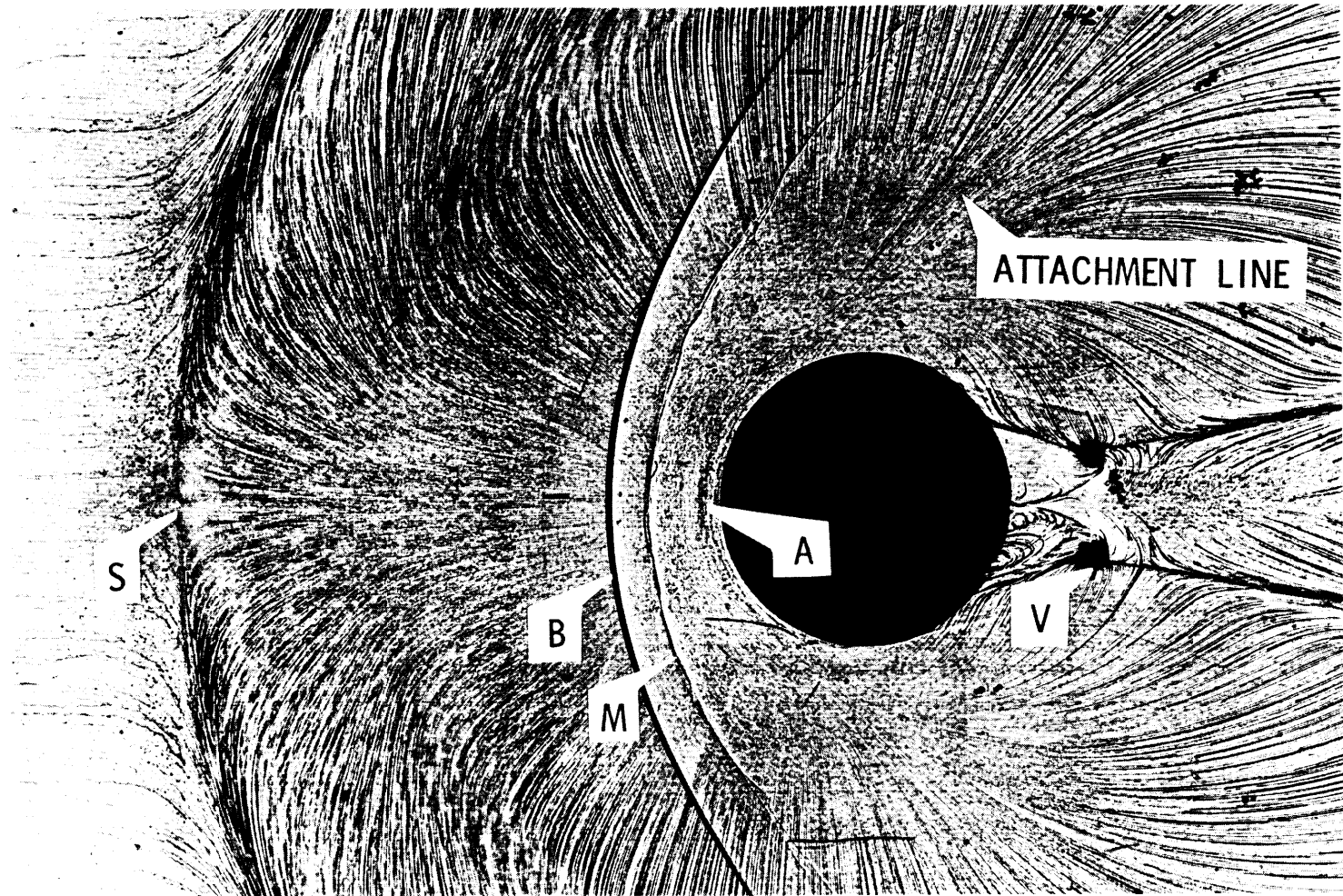Figure 3. Plan-View Shadowgraph for Large Protuberance, Model 2D, M = 2.50, R/ℓ = 19.3x10^6/m. S - Primary Separation, B - Bow Shock, M - Mach Stem, A - Attachment Line, V - Vortex Core. Attachment Line Indicated Originates at Point A.
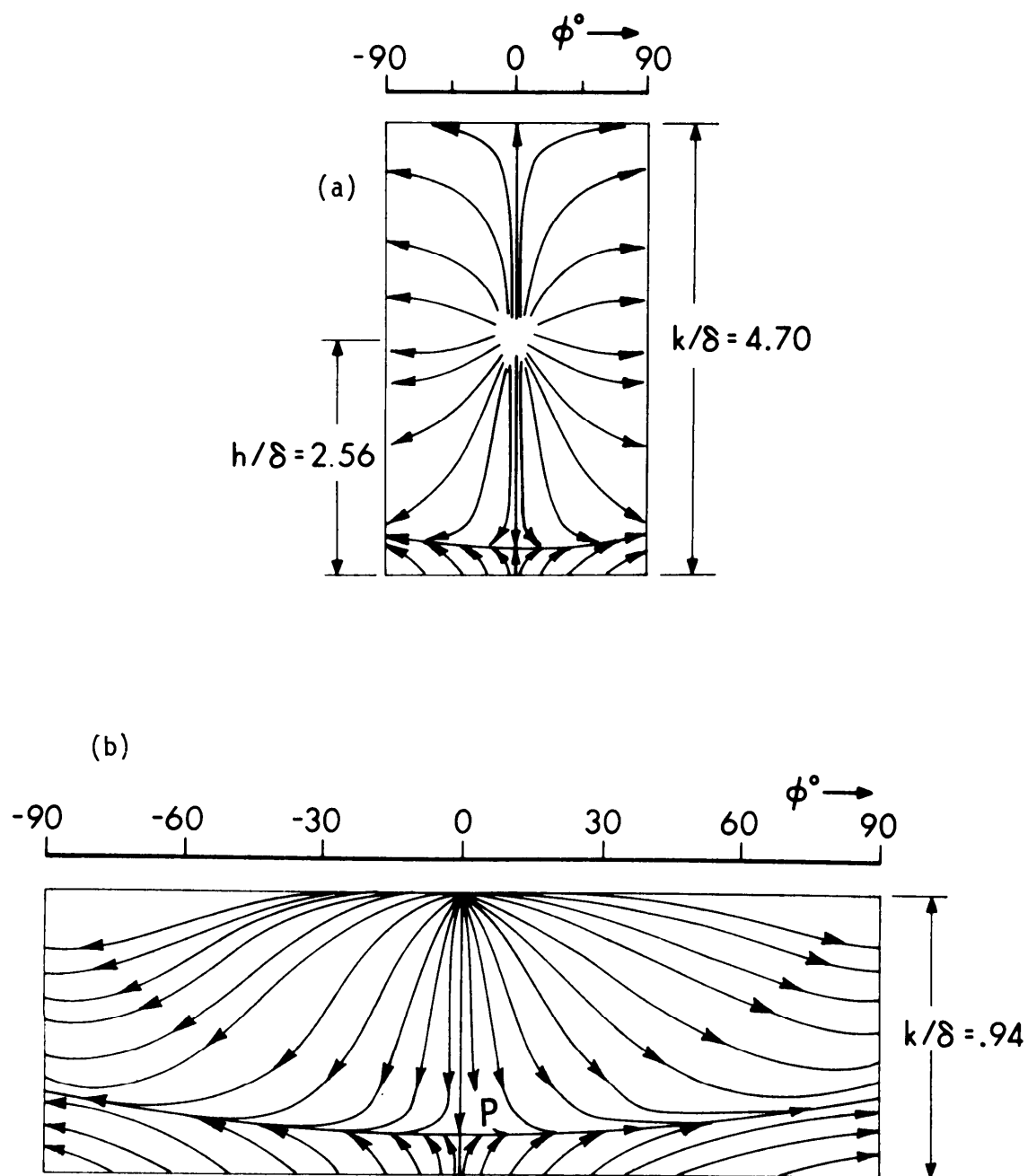
Figure 4.   Sketch of Protuberance Surface Patterns, M = 2.50,
R/ℓ = 9.3x10^6/m, δ = 2.25 cm.   (a) Large Protuberance,
Model 2D; (b) Small Protuberance, Model 2B; Protuber-
ance Leading Edge at ϕ = o.

TOP OF CYLINDRICAL PROTUBERANCE

BOW SHOCK

TRIPLE SHOCK INTERSECTION

M > I

SEPARATION SHOCK

MACH STEM SHOCK

WINDOW BOUNDARY LAYER

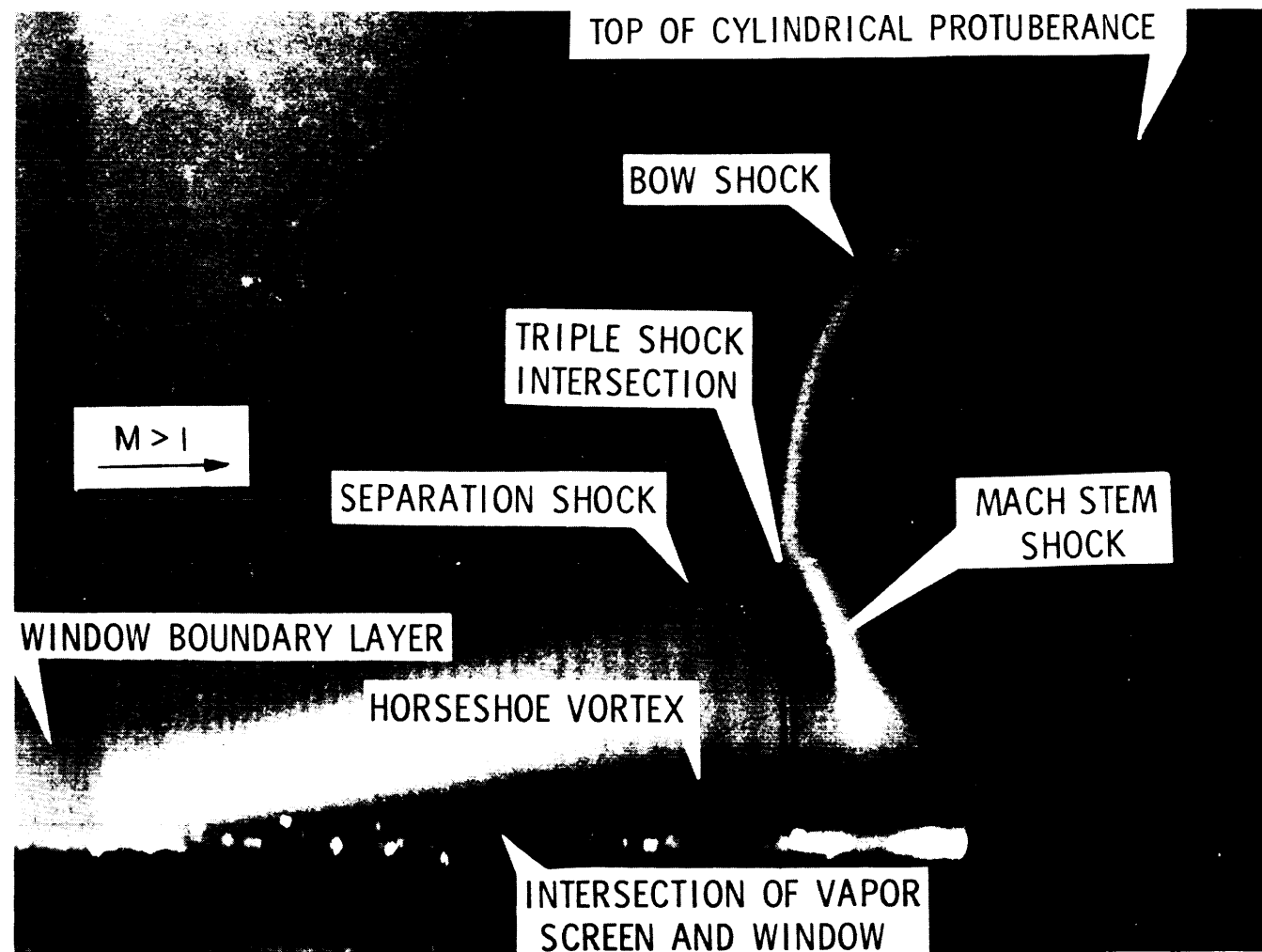HORSESHOE VORTEX

INTERSECTION OF VAPOR SCREEN AND WINDOW

Figure 5.   Vapor Screen Photograph for Large Protuberance, Model 2D, with Light Sheet in Symmetry Plane and Camera at 30° to Sheet, M = 2.50, $R/\ell = 9.3 \times 10^6$/m.
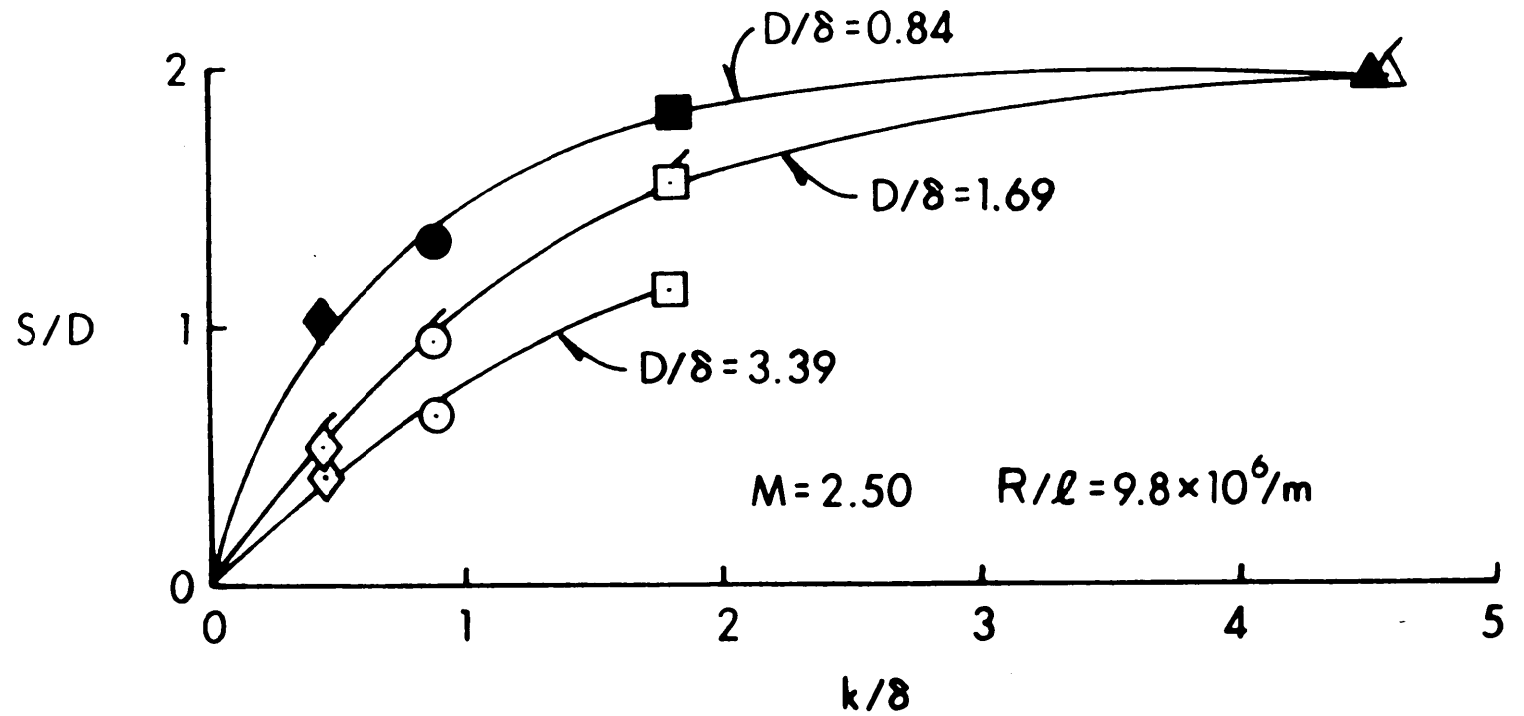
Figure 6. Primary Separation Distance (S/D) vs. Protuberance
Height (k/δ), M = 2.50, R/ℓ = 9.8x10^6/m, δ = 2.25 cm.
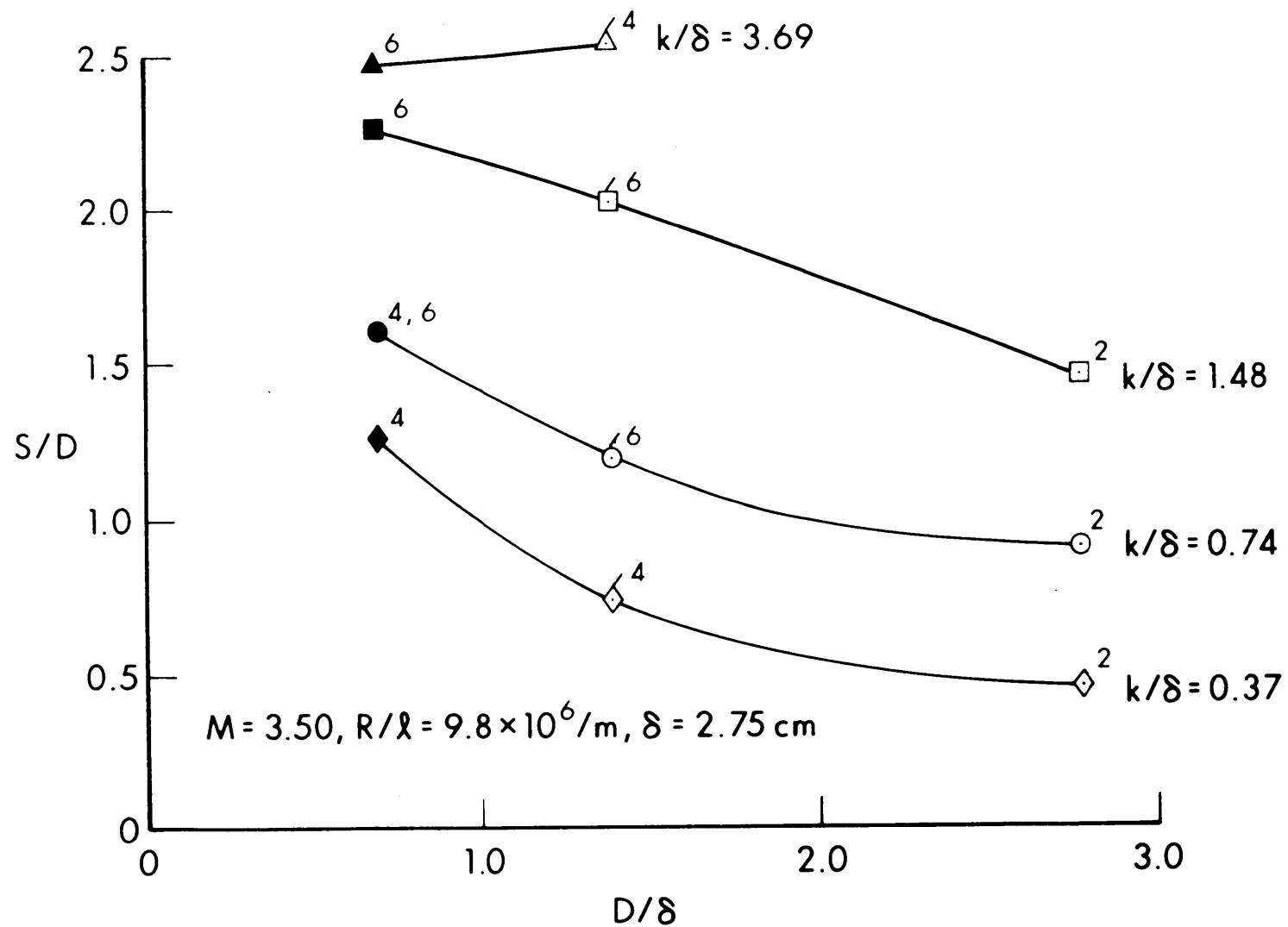
Figure 7. Primary Separation Distance (S/D) vs. Protuberance Diameter (D/δ),
M = 3.50, R/ℓ = 9.8x10^{6}/m, δ = 2.75 cm.

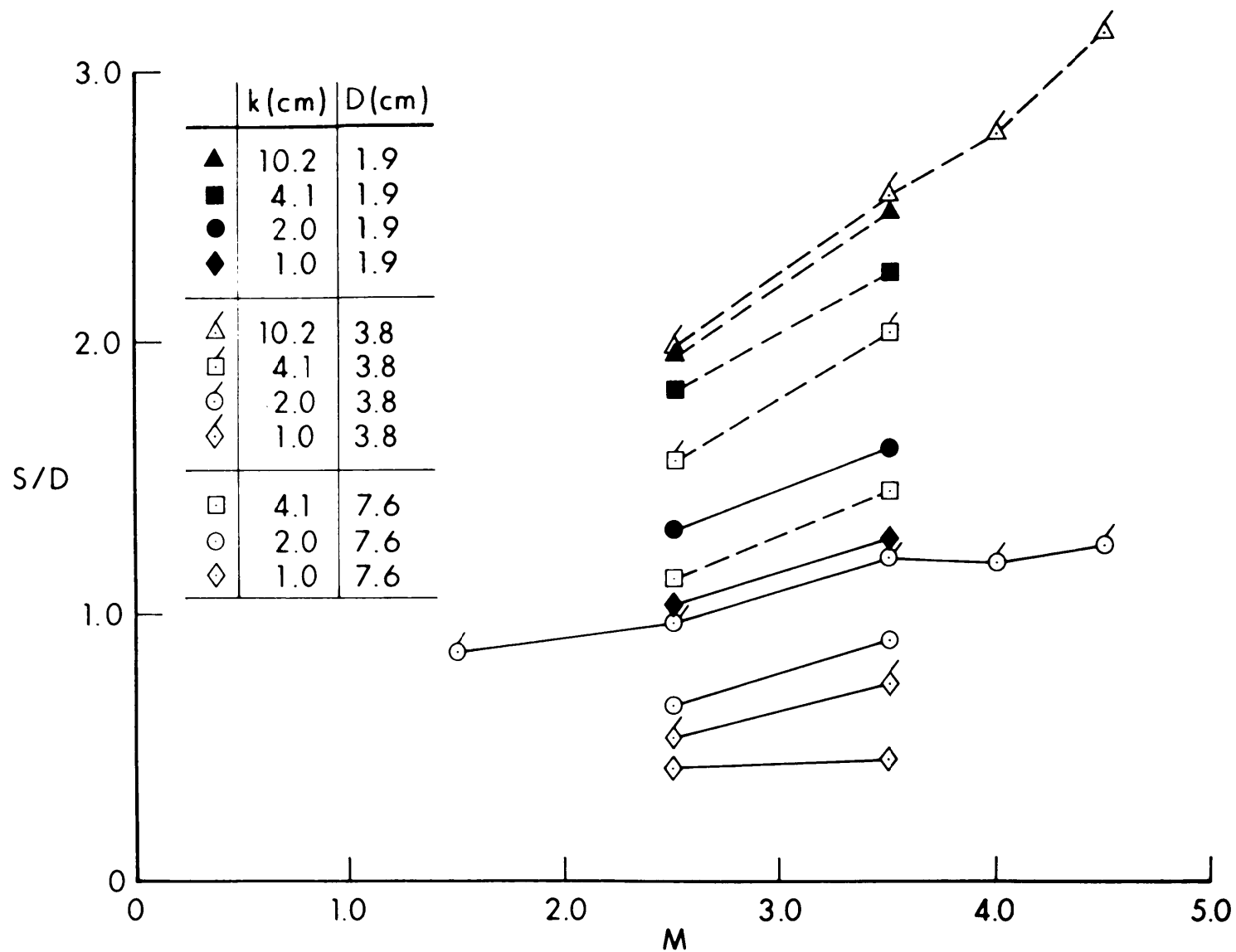|	k(cm)	D(cm)
▲	10.2	1.9
■	4.1	1.9
●	2.0	1.9
◆	1.0	1.9
△	10.2	3.8
⬔	4.1	3.8
◍	2.0	3.8
◇	1.0	3.8
□	4.1	7.6
○	2.0	7.6
◇	1.0	7.6

Figure 8. Primary Separation Distance (S/D) vs. Mach Number (M), $R/\ell = 9.8 \times 10^6/m$.

Figure 9. Primary Separation Distance (S/D) vs. Protuberance Height (k/D), M = 2.50, R/ℓ = 9.8x10^6/m, δ = 2.25 cm. ⊙ - Reference 4; ◄─► 5 Points from Reference 14.
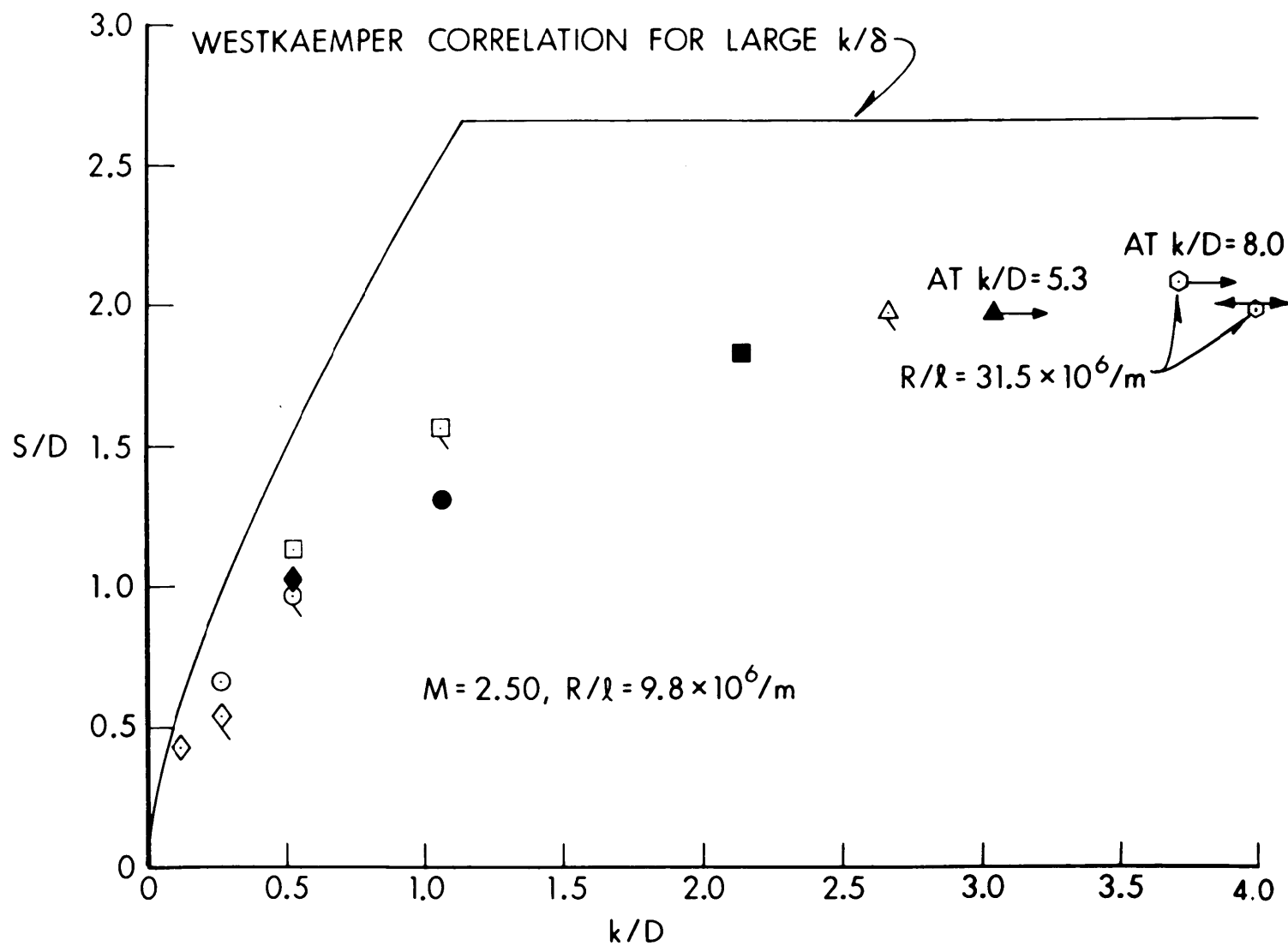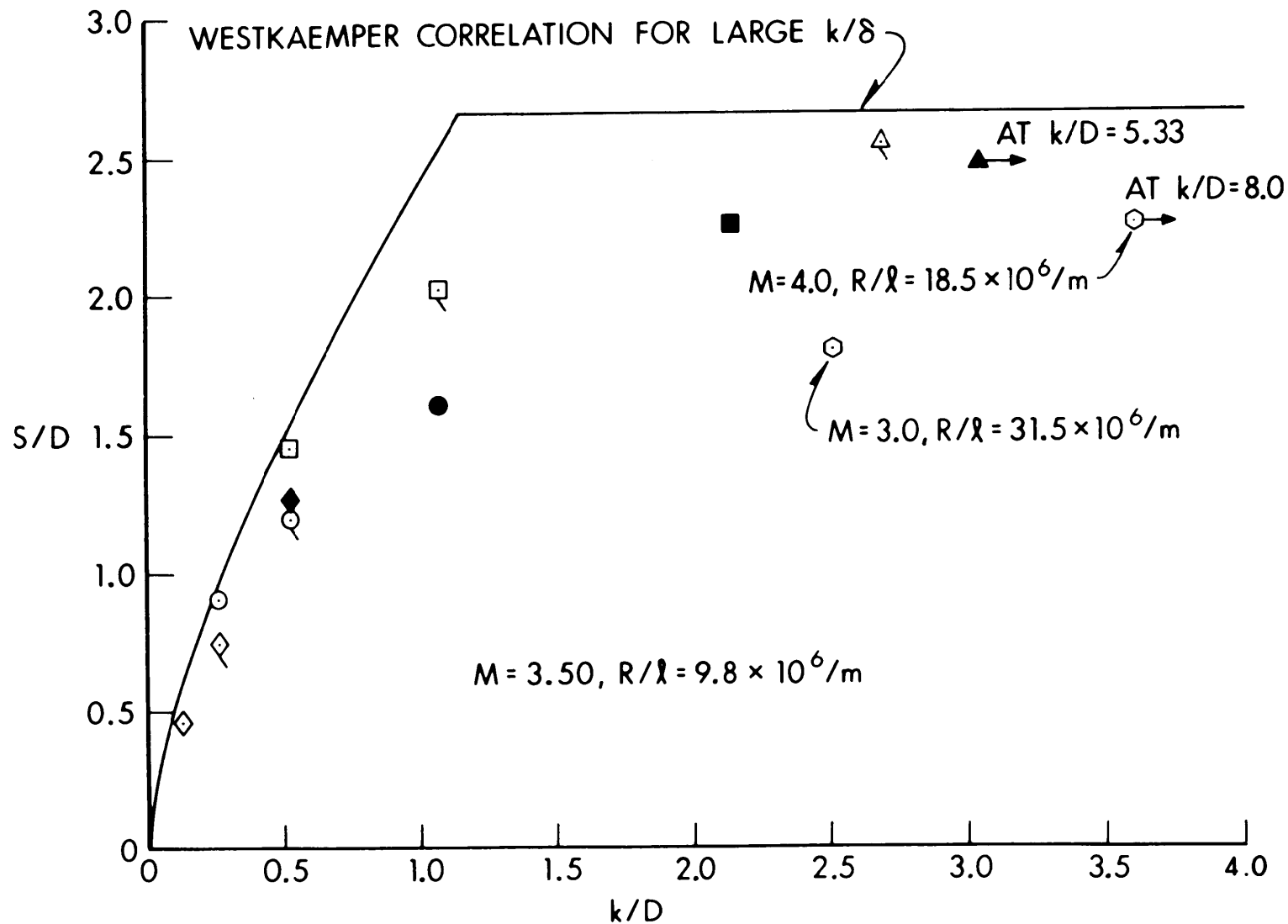
Figure 10. Primary Separation Distance (S/D) vs. Protuberance Height (k/D), M = 3.50, R/ℓ = 9.8x10^{6}/m, δ = 2.75 cm. ⬡ - Reference 4.
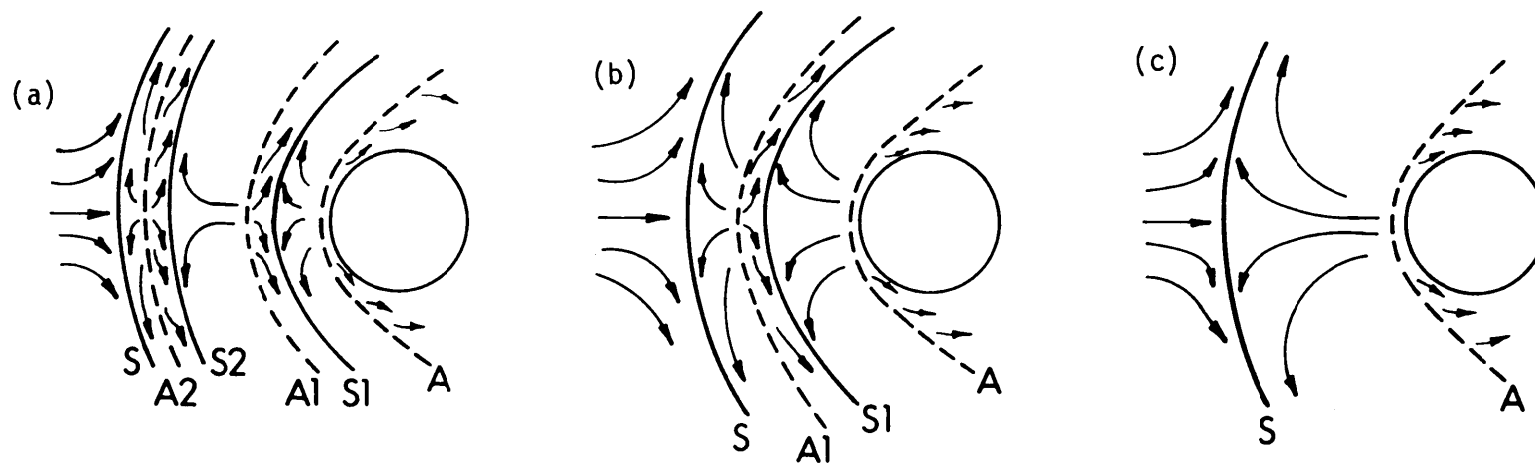
Figure 11. Plan-View Sketches of Separation and Attachment Upstream
of Cylindrical Protuberance as R/ℓ changes; (a) Six Vortices;
(b) Four Vortices; (c) Two Vortices.
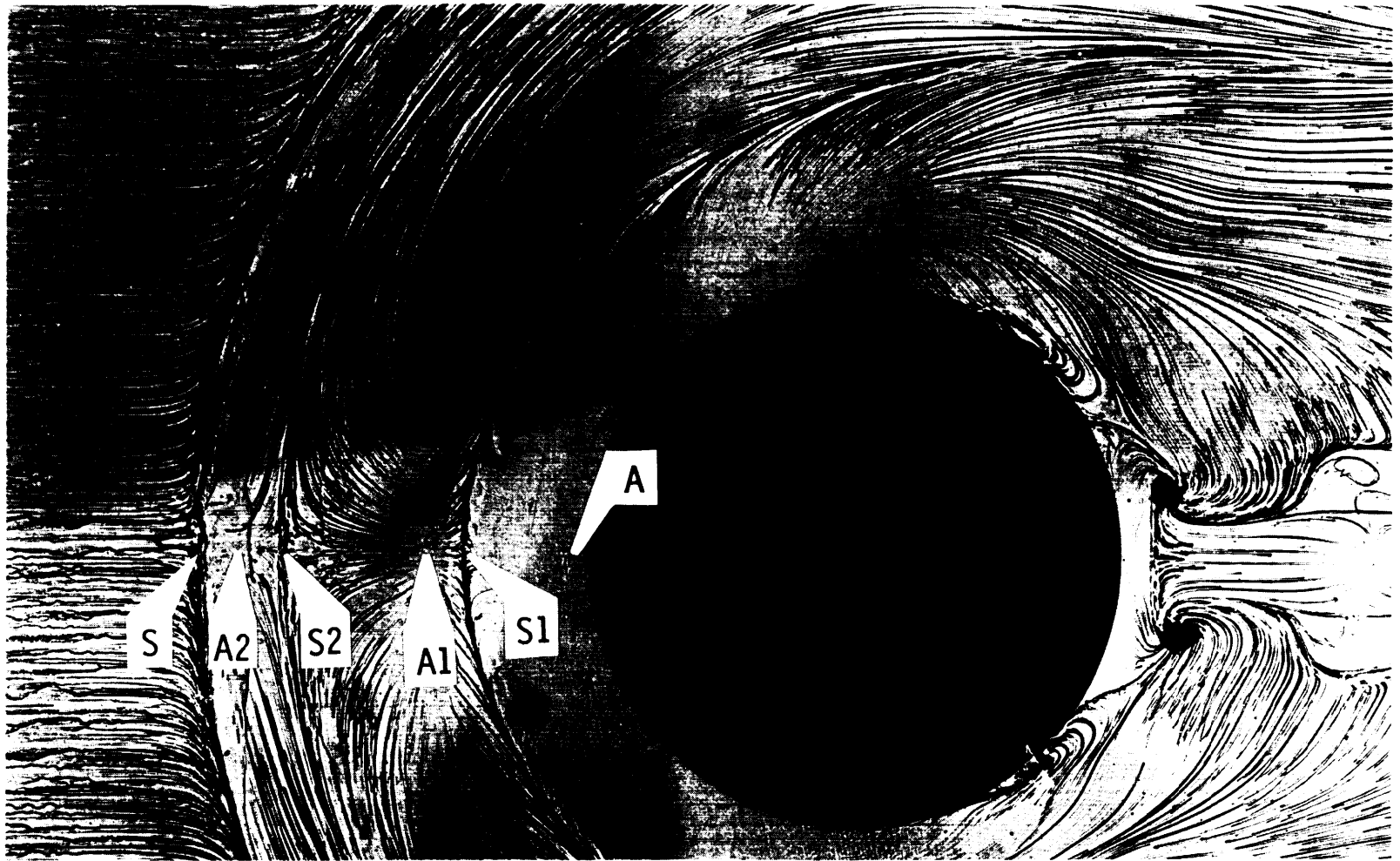
Figure 12. Plan-View Shadowgraph Illustrating Six-Vortex Configuration for Model 3B, $M = 2.50$, $R/\ell = 3.0 \times 10^6/m$. S - Primary Separation; S1, S2 - Secondary Separations; A1, A2 - Attachment Lines.
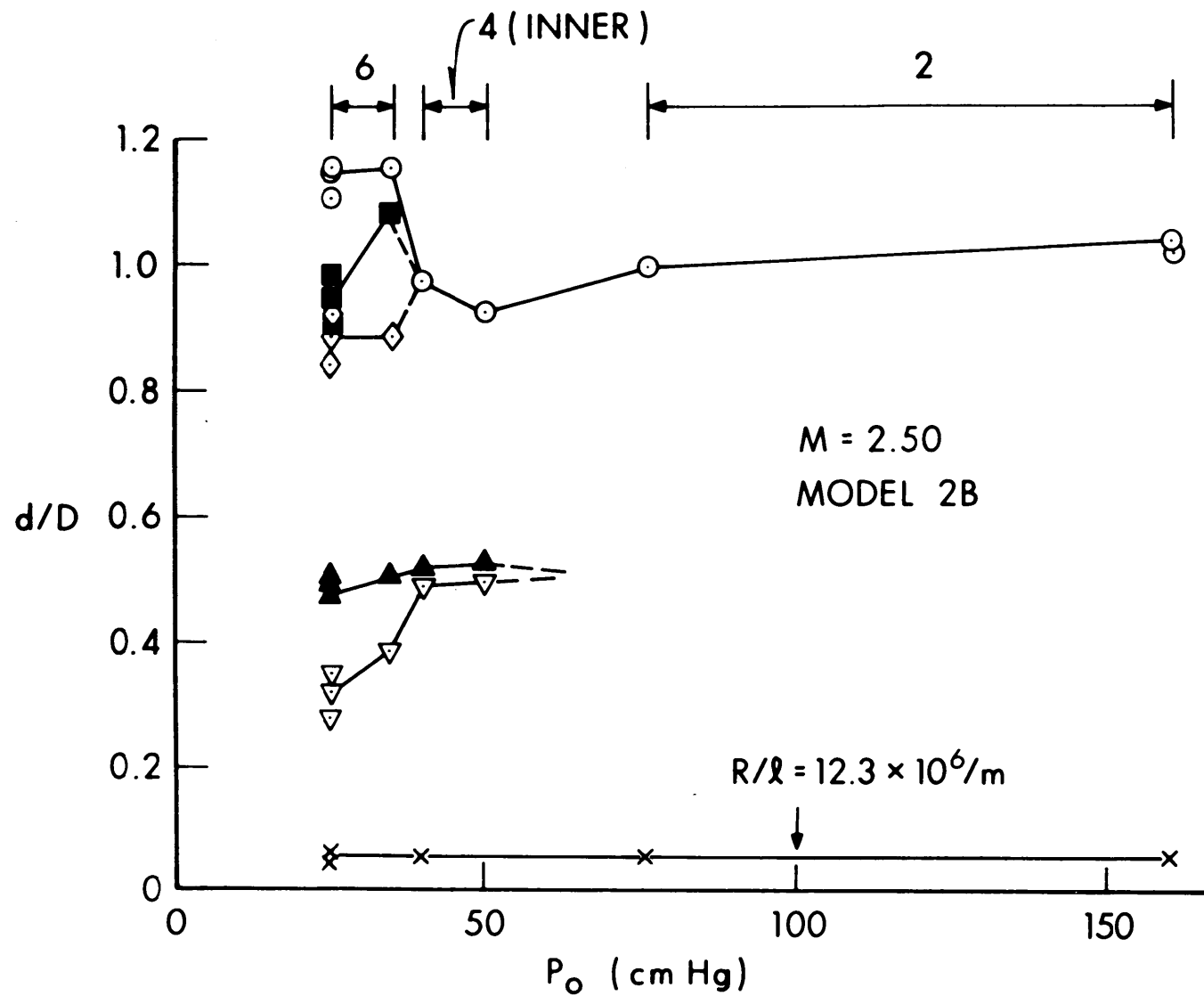
Figure 13. Position of Separation and Attachment Points vs. Stagnation
Pressure (P_o), Model 2B, M = 2.50. Symbols Defined in
Figure 14.
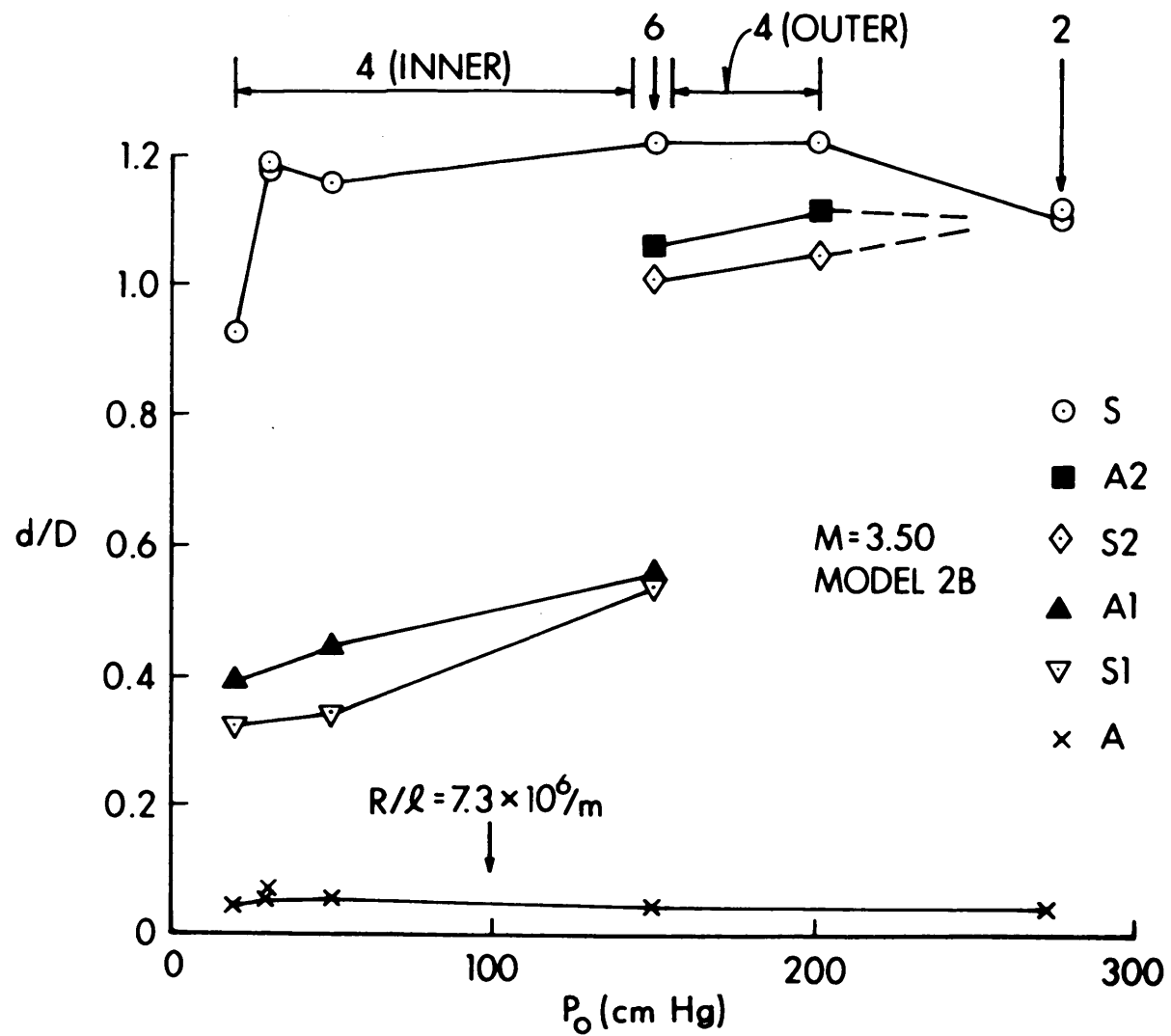
Figure 14. Position of Separation and Attachment Points vs. Stagnation Pressure (P_o), Model 2B, M = 3.50.
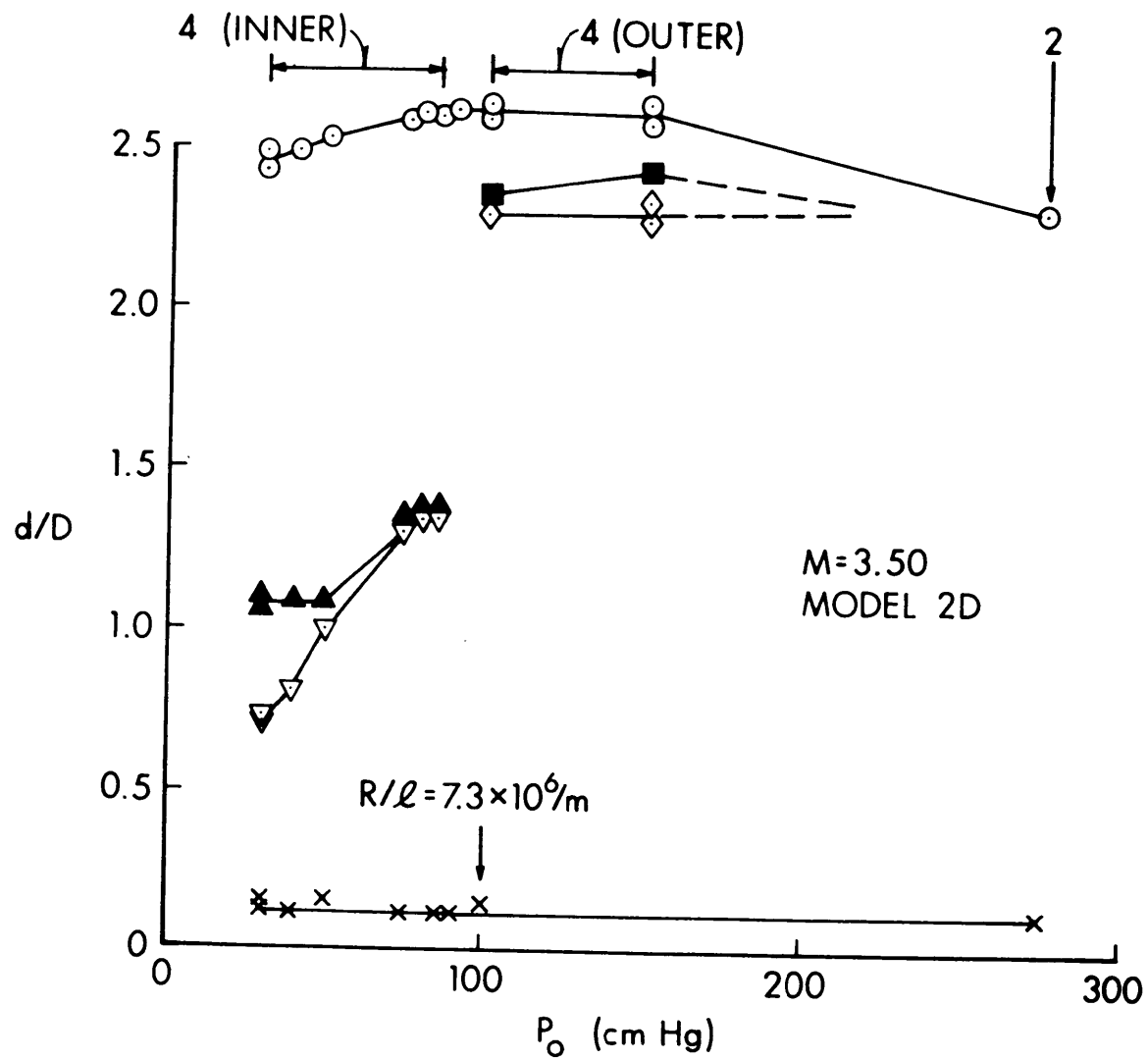
Figure 15. Position of Separation and Attachment Points vs. Stagnation Pressure (P_o), Model 2D, M = 3.50. Symbols Defined in Figure 14.

41
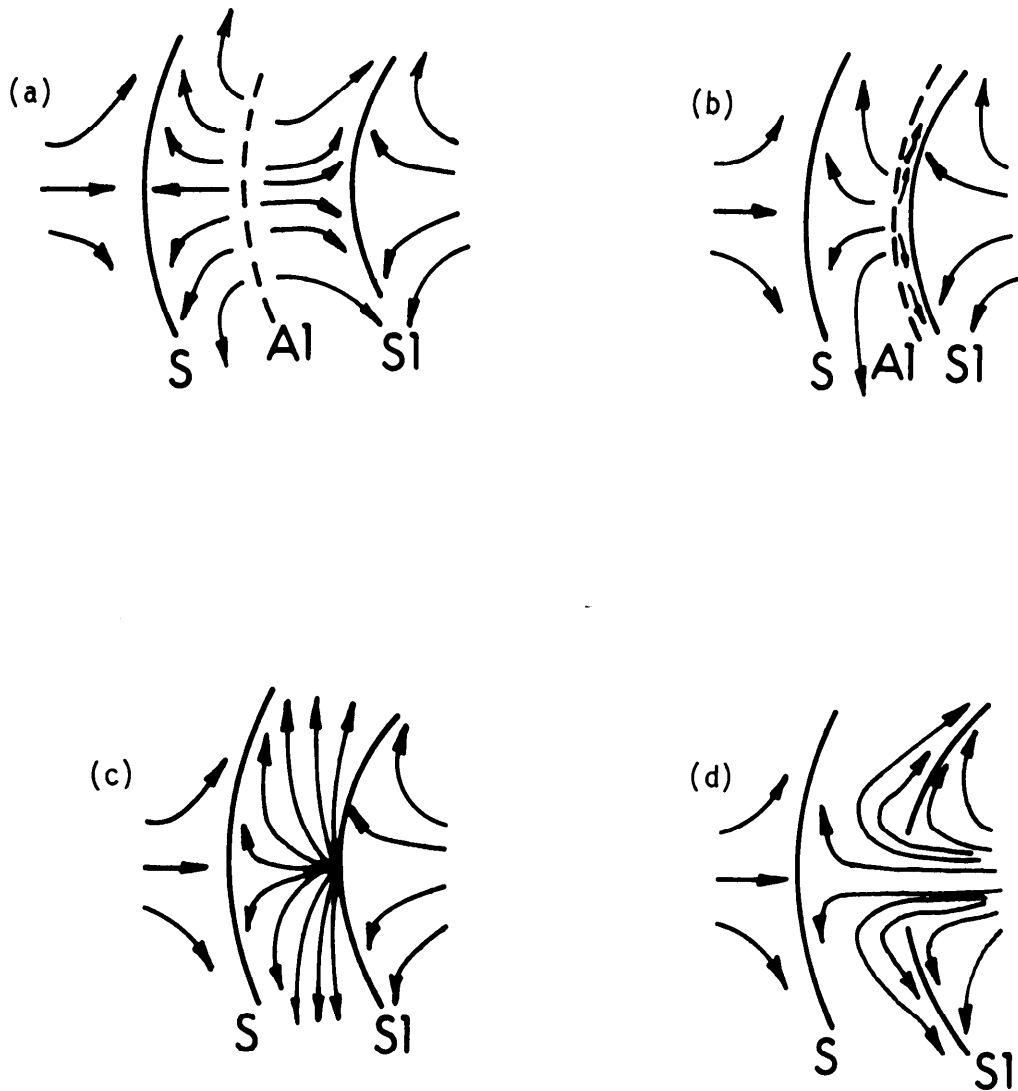
Figure 16.   Plan-View Sketches Showing Merging of Separation and
Attachment Lines.   (a) Secondary Separation S1 Distinct
from Attachment A1; (b) S1 Moves Closer to A1; (c) S1
Merges with A1, Forming One-Half of a Nodal Point of
Attachment; (d) Open-Type of Secondary Separation S1,
with Flow-Through Center.

42

43

Figure 17a.   Side-View in Plane of Symmetry of Small Protuberance Separated Flow
Showing Six-Vortex Configuration; Adapted from Jet-Maze Model of
Reference 9.   For Clarity, Shock Waves Are Omitted and the Horizon-
tal Scale Is Stretched.
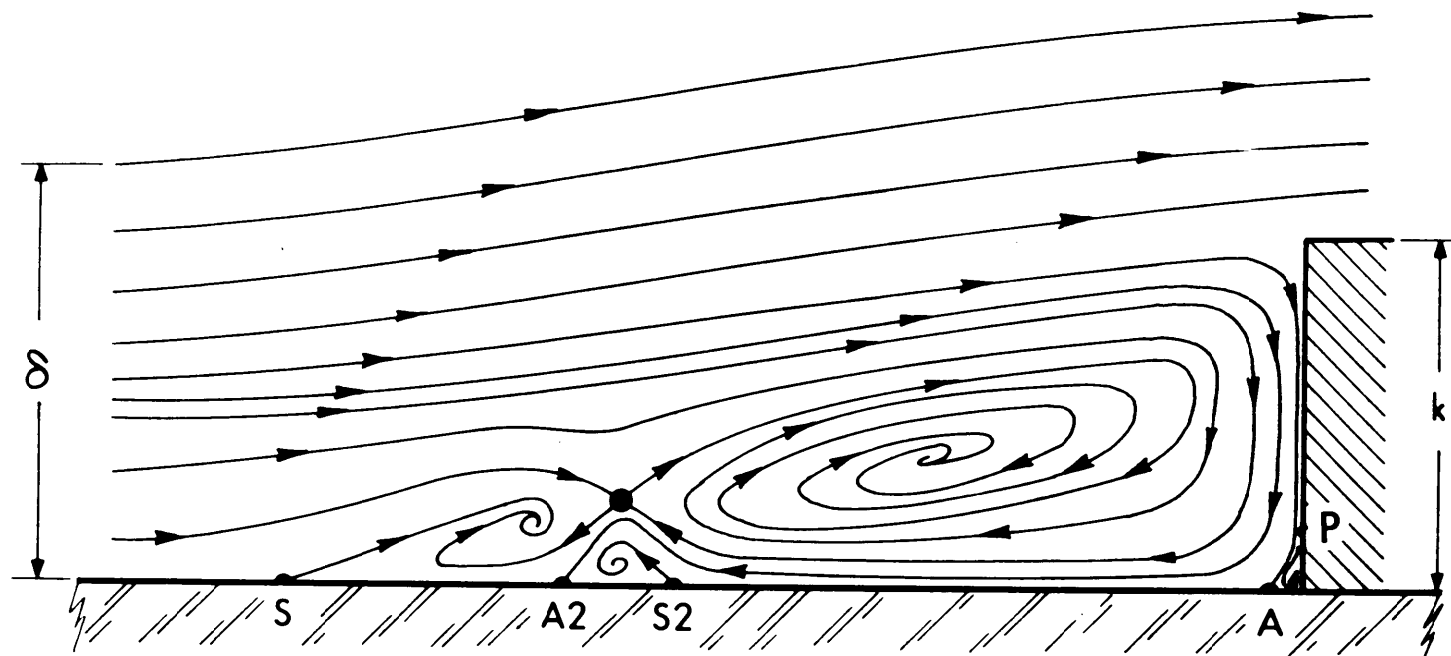
Figure 17b. Side-View in Plane of Symmetry of Small Protuberance Separated Flow Showing Four-Outer Vortex Configuration; Adapted from Jet-Maze Model of Reference 9. For Clarity, Shock Waves Are Omitted and the Horizontal Scale Is Stretched.
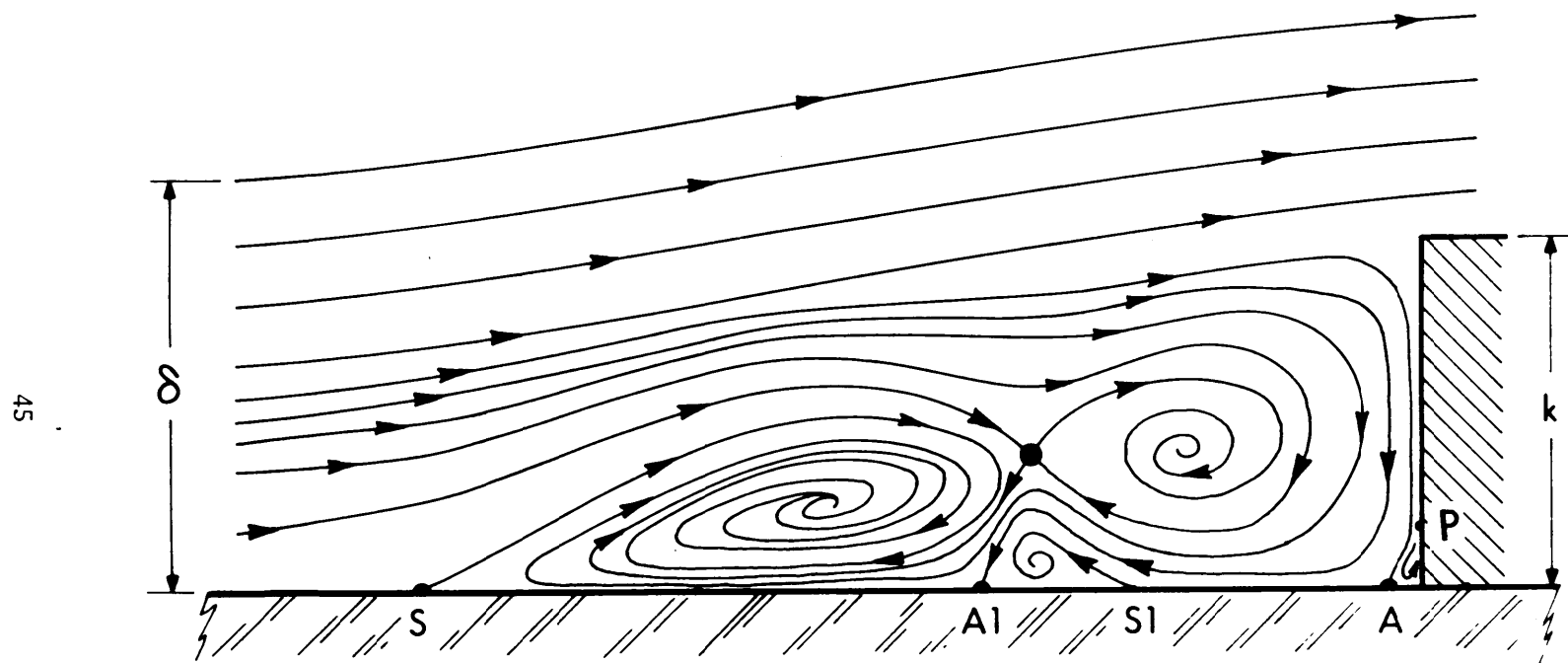
Figure 17c. Side-View in Plane of Symmetry of Small Protuberance Separated Flow
Showing Four-Inner Vortex Configuration; Adapted from Jet-Maze Model
of Reference 9. For Clarity, Shock Waves Are Omitted and the Hori-
zontal Scale Is Stretched.
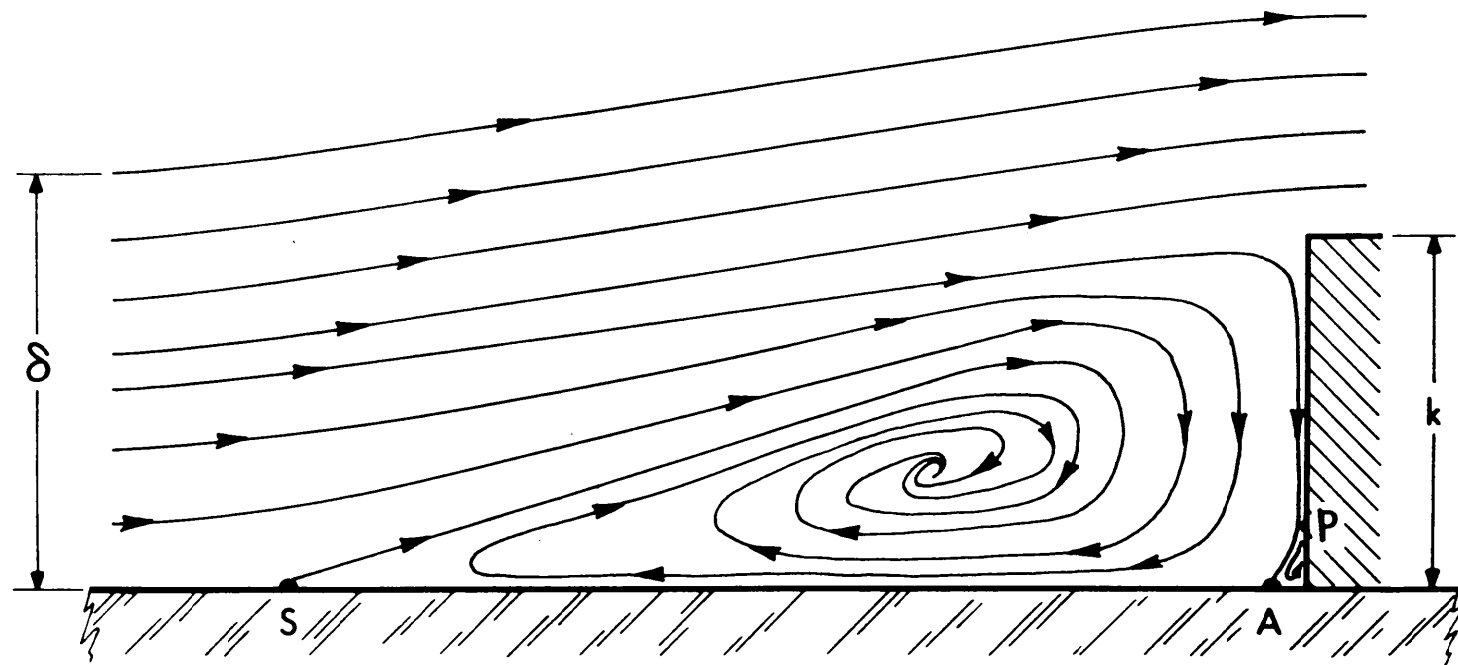
Figure 17d.   Side-View in Plane of Symmetry of Small Protuberance Separated Flow
Showing Two-Vortex Configuration; Adapted from Jet-Maze Model of
Reference 9.   For Clarity, Shock Waves Are Omitted and the Horizon-
tal Scale Is Stretched.
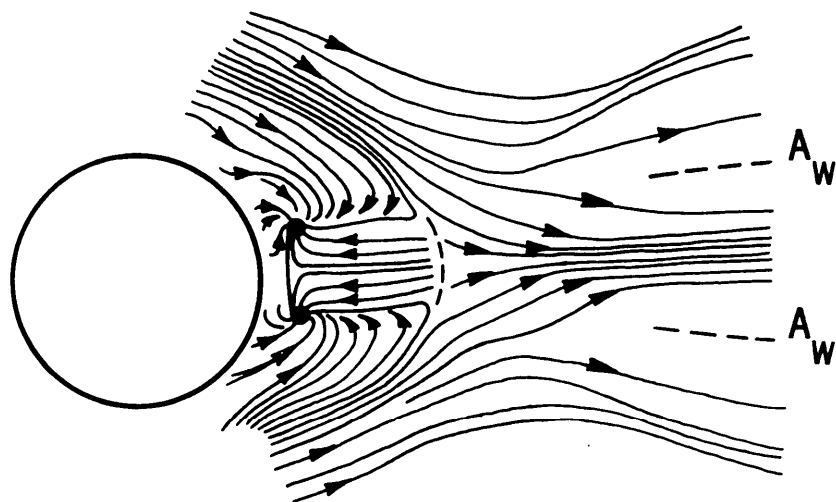
Figure 18. Plan-View Sketch of Near Wake for Small Protu-
berance, Model 2B, M = 3.50, R/ℓ = 19.9x10^6/m.
Separation Line Downstream in Symmetry Plane.

47
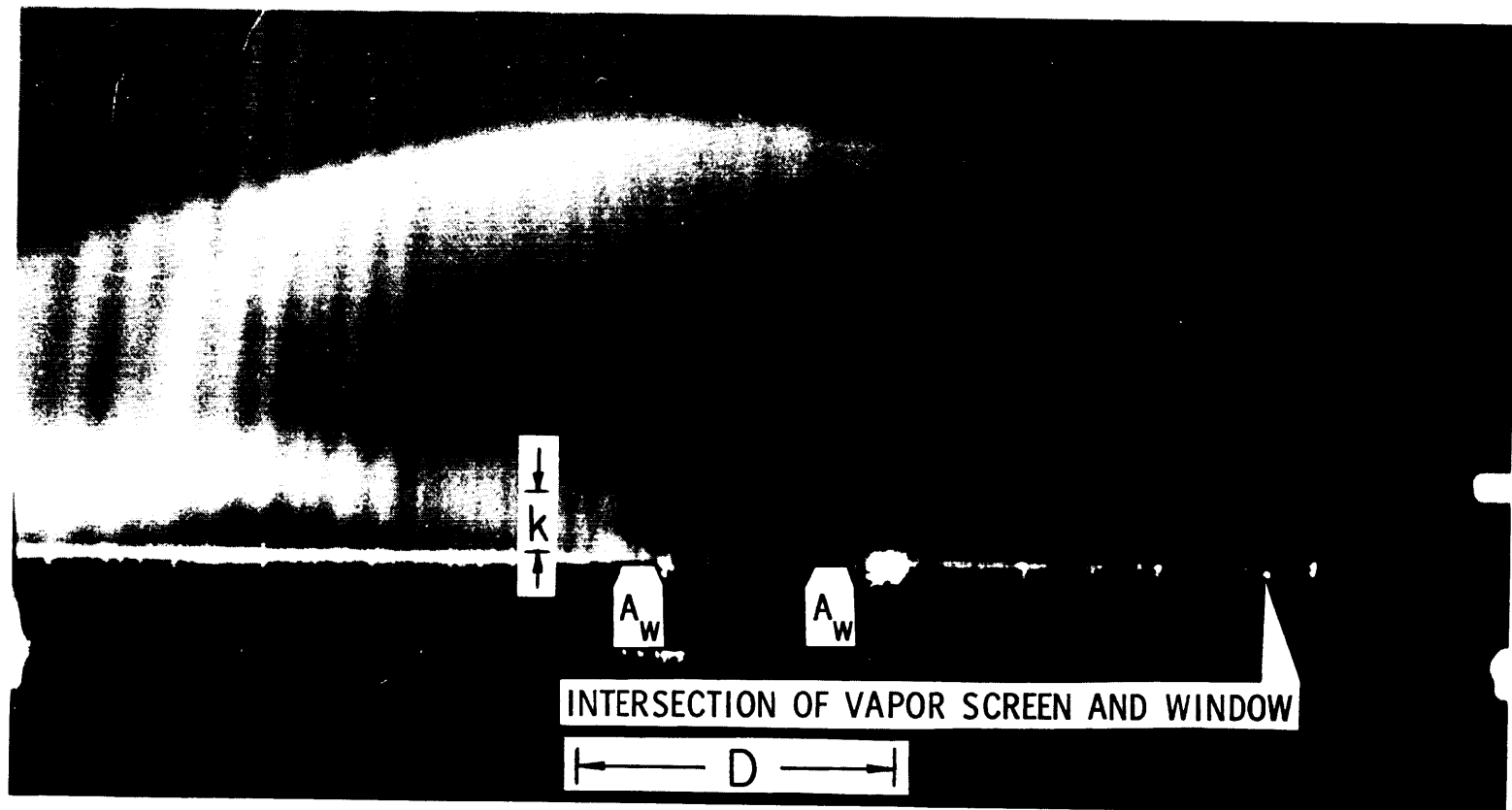
Figure 19. Vapor Screen Photograph for Small Protuberance, Model 2B, with Light Sheet Normal to the Surface and Free Stream. Sheet Is 2.0 Diameters Downstream of the Cylinder Leading Edge, $M = 2.50$, $R/\ell = 9.3 \times 10^6$/m. A_W Attachment Line in Oil Surface Pattern.
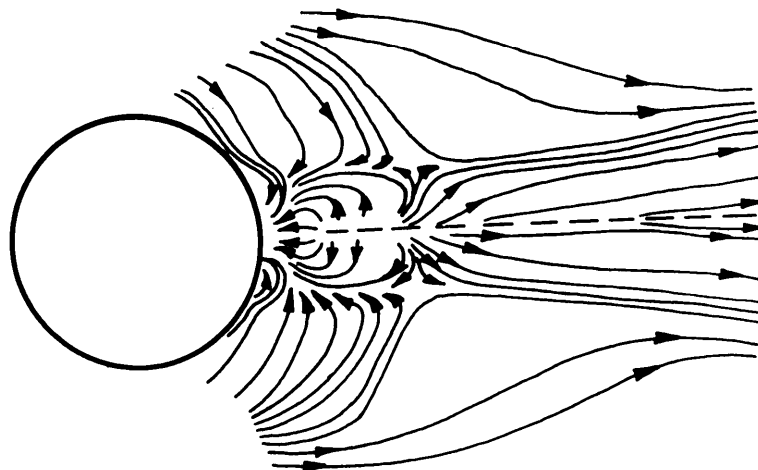
Figure 20. Plan-View Sketch of Near Wake for Large Protu-
berance, Model 2D, M = 3.50, R/ℓ = 19.9x10^6/m.
Attachment Line Downstream in Symmetry Plane.

49
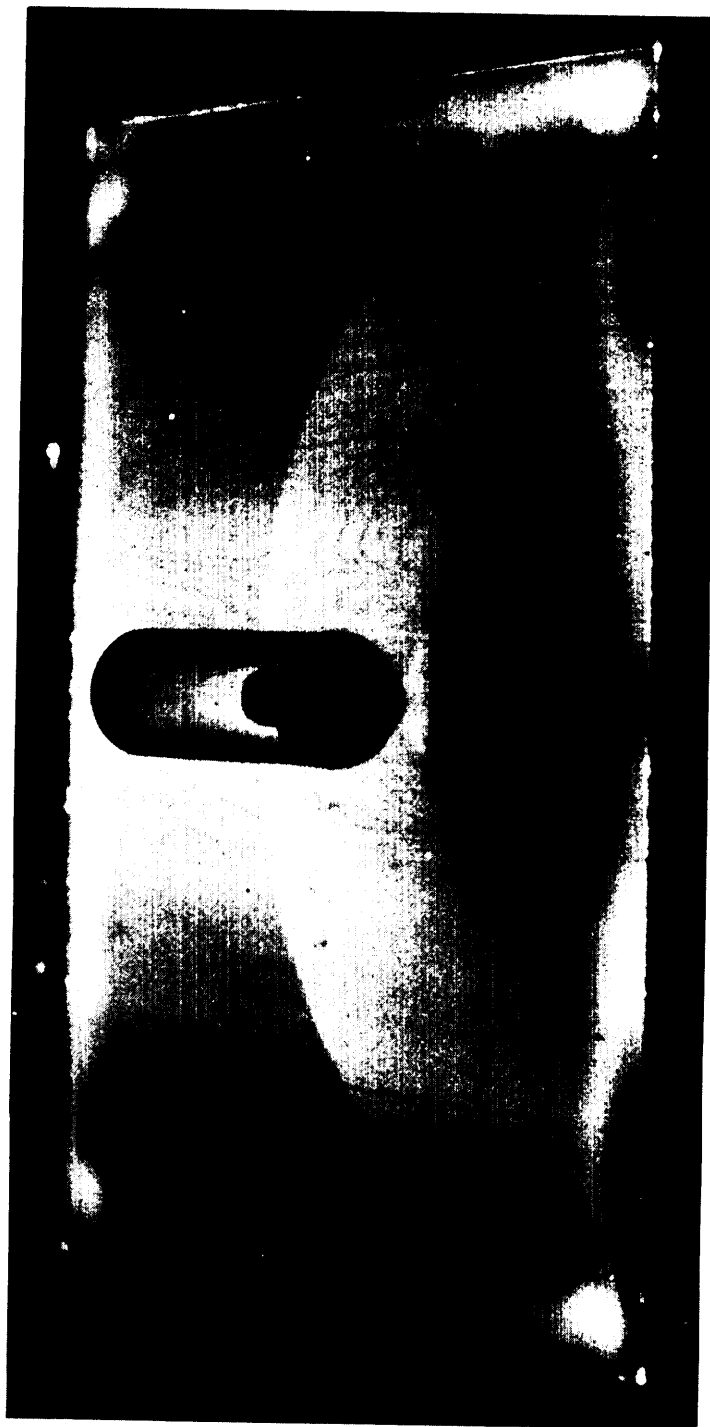
Figure 21. Vapor Screen View of the Wake Looking Downstream,
from Below; Light Sheet at 3 Diameters Downstream.
Model 2D, M = 2.50, R/ℓ = 9.3×10^6/m

REFERENCES

1. R. Sedney, "A Survey of the Effects of Small Protuberances on
    Boundary Layer Flows," AIAA Journal, Vol. 11, No. 6, June 1973,
    pp. 782-792.

2. R. Greeley, J. D. Iversen, J. B. Pollack, N. Udovich and B. White,
    "Wind Tunnel Studies of Martian Aeolian Processes," Proc. Roy. Soc.
    Lond. A., Vol. 341, No. 1626, 10 December 1974, pp. 331-360.
    See also "Wind Tunnel Simulations of Light and Dark Streaks on
    Mars," Science, Vol. 183, March 1974, pp. 847-849.

3. R. H. Korkegi, "Survey of Viscous Interaction Associated with High
    Mach Number Flight," AIAA Journal, Vol. 9, No. 5, May 1971, pp.
   771-784.

4. L. G. Kaufman II, R. H. Korkegi and L. C. Morton, "Shock Impinge-
    ment Caused by Boundary-Layer Separation Ahead of Blunt Fins,"
    AIAA Journal, Vol. 11, No. 10, October 1973, pp. 1363-1364.
    See also ARL 72-0118, Aerospace Research Laboratories, August 1972.

5. J. C. Westkaemper, "Turbulent Boundary-Layer Separation Ahead of
    Cylinders," AIAA Journal, Vol. 6, No. 7, July 1968, pp. 1352-1355.

6. R. Sedney, "Visualization of Boundary Layer Flow Patterns Around
    Protuberances Using an Optical-Surface Indicator Technique," The
    Physics of Fluids, Vol. 15, No. 12, December 1972, pp. 2439-2441.

7. R. Sedney, C. W. Kitchens, Jr., and C. C. Bush, "The Marriage of
    Optical, Tracer, and Surface Indicator Techniques in Flow Visuali-
    zation - A Survey," Record of the 1973 International Congress on
    Instrumentation in Aerospace Simulation Facilities, IEEE Publica-
    tion No. 73CHO 784-9AES, pp. 155-171.

8. A. E. Winkelmann, "Flow Visualization Studies of a Fin Protuber-
    ance Partially Immersed in a Turbulent Boundary Layer at Mach 5,"
    NOLTR 70-93, Naval Ordnance Laboratory, May 1970.

9. R. S. Norman, "On Obstacle Generated Secondary Flows in Laminar
    Boundary Layers and Transition to Turbulence," Ph.D. Thesis,
    Illinois Institute of Technology, December 1972.

10. R. L. Maltby, "Flow Visualization in Wind Tunnels Using Indicators,"
    AGARD-ograph 70, AGARD-NATO Fluid Dynamics Panel, 1962.

11. D. M. Voitenko, A. I. Zubkov and Y. A. Panov, "Existence of Super-
    sonic Zones in Three-Dimensional Separation Flows," Izv. AN SSSR.
    Mekhanika Zhidkosti i Gaza, Vol. 2, No. 1, 1967, pp. 20-24.

12. Private communication from R. K. Matthews, Arnold Engineering and Development Center, to C. J. Nietubicz, Ballistic Research Laboratories, 1972 and 1973.

13. E. A. Price and R. L. Stallings, "Investigation of Turbulent Separated Flows in the Vicinity of Fin-Type Protuberances at Supersonic Mach Numbers," NASA TN D-3804, February 1967.

14. D. M. Voitenko, A. I. Zubkov and Y. A. Panov, "Supersonic Gas Flow Past a Cylindrical Obstacle on a Plate," Mekhanika Zhidkosti i Gaza, Vol. 1, No. 1, 1966, pp. 121-125.

15. E. C. Maskell, "Flow Separation in Three Dimensions," Rept. No. Aero 2565, Royal Aircraft Establishment, Farnborough, November 1955.

16. M. V. Morkovin, "An Approach to Flow Engineering via Functional Flow Modules," Beiträge zur Strömungsmechanik, insbesondere zur Grenzschichttheorie, Porz-Wahn, DLR F Vol. 2, pp. 270-301, 1972.

17. N. Gregory and W. S. Walker, "The Effect on Transition of Isolated Surface Excrescences in the Boundary Layer," R & M 2779, Pt. I, 1955, Aeronautical Research Council, England.

LIST OF SYMBOLS

d   distance from protuberance leading edge to attachment or separation position in flow symmetry plane, see Figures 13 - 15, m

h   distance from base of large cylindrical protuberance to attachment point on leading edge in Figure 4, m

k   obstacle height, m

A   distance from cylinder leading edge to attachment position of small vortex in flow symmetry plane, m

A_1, A_2 distance from cylinder leading edge to attachment position in flow symmetry plane as in Figure 17, m

A_w position of attachment line in near wake of small protuberance shown in Figures 18 and 19, nondimensional

D   diameter of cylindrical protuberance, m

M   freestream Mach number, nondimensional

P   position of separation point on leading edge of small cylindrical protuberance shown in Figures 4b and 17, nondimensional

P_o freestream stagnation (supply) pressure, cm-Hg or N/m^2

R/ℓ unit Reynolds number based on freestream velocity ($= U_\infty/\nu$), m^{-1}

R_D Reynolds number based on cylinder diameter and freestream velocity ($= U_\infty D/\nu$), nondimensional

R_k Reynolds number based on cylinder height and freestream velocity ($= U_\infty k/\nu$), nondimensional

S   distance from protuberance leading edge to position of primary separation in flow symmetry plane, m

S_1, S_2 distance from cylinder leading edge to secondary separation position in flow symmetry plane as in Figure 17, m

U_k undisturbed velocity at height k off surface, m/s

U_∞ freestream velocity, m/s

δ boundary layer thickness defined by 99% of freestream velocity, m

ν kinematic viscosity, m^2/sec

Δ bow shock detachment distance for cylindrical protuberance, m

53

DISTRIBUTION LIST

No. of Copies	Organization	No. of Copies	Organization

12   Commander
Defense Documentation Center
ATTN: DDC-TCA
Cameron Station
Alexandria, VA 22314

2   Commander
US Army Materiel Command
ATTN: AMCDMA, Mr. N. Klein
          Mr. J. Bender
5001 Eisenhower Avenue
Alexandria, VA 22333

1   Commander
US Army Materiel Command
ATTN: AMCRD, BG H.A. Griffith
5001 Eisenhower Avenue
Alexandria, VA 22333

1   Commander
US Army Materiel Command
ATTN: AMCRD-T
5001 Eisenhower Avenue
Alexandria, VA 22333

1   Commander
US Army Aviation Systems
  Command
ATTN: AMSAV-E
12th and Spruce Streets
St. Louis, MO 63166

1   Director
US Army Air Mobility Research
  and Development Laboratory
Ames Research Center
Moffett Field, CA 94035

1   Commander
US Army Electronics Command
ATTN: AMSEL-RD
Fort Monmouth, NJ 07703

2   Commander
US Army Missile Command
ATTN: AMSMI-R
      Ray Deep
Redstone Arsenal, AL 35809

1   Commander
US Army Tank Automotive Command
ATTN: AMSTA-RHFL
Warren, MI 48090

3   Commander
US Army Mobility Equipment
  Research & Development Center
ATTN: AMSME-HKF, Ashok Patil
     Tech Docu Cen, Bldg. 315
     AMSME-RZT
Fort Belvoir, VA 22060

1   Commander
US Army Armament Command
Rock Island, IL 61202

1   Commander
US Army Picatinny Arsenal
ATTN: SARPA-FR-S-A, A. Loeb
Dover, NJ 07801

1   Commander
US Army Harry Diamond
  Laboratories
ATTN: AMXDO-TI
2800 Powder Mill Road
Adelphi, MD 20783

3   Commander
US Naval Air Systems Command
ATTN: AIR-604
Washington, DC 20360

DISTRIBUTION LIST

No. of Copies	Organization

3	Commander
	U.S. Naval Ordnance Systems
	   Command
	ATTN: ORD-0632
	       ORD-035
	       ORD-5524
	Washington, DC 20360

1	Commander U.S. Naval Ship Research and Development Center ATTN: Tech. Library Washington, DC 20007

1	Commander
	U.S. Naval Ship Research
	   and Development Center
	ATTN: S. de los Santos
	       Head, High Speed
	       Aero. Div.
	Bethesda, Maryland 20034

4	Commander
	Naval Surface Weapons Center
	Applied Aerodynamics Division
	  (Code 312)
	White Oak
	ATTN: K. Lobb
	       S. M. Hastings
	       A. E. Winklemann
	       W. C. Ragsdale
	Silver Spring, Maryland 20910

1	Commander US Naval Surface Weapons Center ATTN: Tech. Library Dahlgren, VA 22448
1	AFATL (DLR) Eglin AFB Florida 32542
1	AFATL (DLRD) Eglin AFB Florida 32542

No. of Copies	Organization
1	AFATL (DLRV) Elgin AFB Florida 32542

4	Director
	NASA Ames Research Center
	ATTN: J. Rakich
	       J. Marvin
	       B. Wick
	       Tech. Library
	Moffett Field, CA 94035

6	Director
	NASA Langley Research Center
	ATTN: D. Bushnell
	       R. Trimpi
	       J. South
	       E. Price
	       J. R. Sterrett
	       Tech. Library
	Langley Station
	Hampton, Virginia 23365

1	Director NASA Lewis Research Center ATTN: MS 60-3, Tech. Lib. 21000 Brookpark Road Cleveland, Ohio 44135

1	Director
	NASA Marshall Space Flight
	   Center
	ATTN: A. R. Felix, Chief
	       S&E-AERO-AE
	Huntsville, Alabama 35812

2	Director Jet Propulsion Laboratory ATTN: J. Kendall Tec. Lib. 4800 Oak Grove Drive Pasadena, California 91103

DISTRIBUTION LIST

No. of Copies	Organization	No. of Copies	Organization
2	ARL ATTN: R. H. Korkegi J. S. Shang Bldg. 450, Area B Wright-Patterson AFB Ohio 45433	1	General Electric Company ATTN: H. T. Nagamatsu Research & Development Lab (Comb. Bldg.) Schenectady, New York 12301
3	ARO, Inc. ATTN: J. D. Whitfield R. K. Matthews Tech. Lib. Arnold AFS, Tennessee 37389	1	Grumman Aerospace Corp. ATTN: R. E. Melnik Research Dept. Bethpage, New York 11714
1	Aerospace Corporation ATTN: R. L. Varwig Aerophysics Lab. P. O. Box 92957 Los Angeles, CA 90009	2	Lockheed-Georgia Company ATTN: B. H. Little, Jr. G. A. Pounds Dept. 72-74, Zone 403 86 South Cobb Drive Marietta, Georgia 30062
1	AVCO Systems Division ATTN: B. Reeves 201 Lowell Street Wilmington, MA 01887	1	Lockheed Missiles and Space Company ATTN: Tech Information Center 3251 Hanover Street Palo Alto, California 94304
1	The Boeing Company Commercial Airplane Group ATTN: W. A. Bissell, Jr. M.S. 1W-82, Org. 6-8340 Seattle, WA 98124	1	Martin-Marietta Laboratories ATTN: S. H. Maslen 1450 S. Rolling Road Baltimore, Maryland 21227
1	Calspan Corporation ATTN: A. Ritter P. O. Box 235 Buffalo, New York 14221	2	McDonnell Douglas Astronautics Corporation ATTN: J. Xerikos H. Tang 5301 Bolsa Avenue Huntington Beach, CA 92647
1	Center for Interdisciplinary Programs ATTN: Victor Zakkay W. 177th St. & Harlem River Bronx, New York 10453	1	McDonnell Douglas Research Laboratories ATTN: R. Hakkinen Manager - Research Flight Sciences Dept. 222, Bldg. 33
1	General Dynamics ATTN: Research Library 2246 P. O. Box 748 Fort Worth, Texas 76101		P. O. Box 516 St. Louis, Missouri 63166

DISTRIBUTION LIST

No. of Copies	Organization	No. of Copies	Organization
1	Northrup Corporation Aircraft Division ATTN: S. Powers 3901 West Broadway Hawthorne, CA 90250	1	The Johns Hopkins University ATTN: Tech. Library Baltimore, Maryland 21218
1	Sandia Corporation ATTN: Tech. Library P. O. Box 5800 Albuquerque, NM 87115	1	Massachusetts Institute of Technology ATTN: Tech. Library 77 Massachusetts Avenue Cambridge, MA 02139
1	United Aircraft Corporation Research Laboratories ATTN: Library East Hartford, CT 06108	1	North Carolina State University Mechanical and Aerospace Engineering Department ATTN: F. F. DeJarnette Raleigh, North Carolina 27607
1	Vought Systems Division LTV Aerospace Corporation ATTN: J. M. Cooksey Chief, Gas Dynamics Lab., 2-53700 P. O. Box 5907 Dallas, Texas 75222	1	Notre Dame University ATTN: T. J. Mueller Dept. of Aero Engr South Bend, Indiana 46556
1	California Institute of Technology Aeronautics Department ATTN: Tech. Library 1201 East California Blvd. Pasadena, CA 91102	2	Ohio State University Department of Aeronautical & Astronautical Engineering ATTN: S. L. Petrie Tech. Library Columbus, Ohio 43210
1	California Institute of Technology Guggenheim Aeronautical Lab. ATTN: Tech. Library Pasadena, CA 91104	2	Princeton University James Forrestal Research Center Gas Dynamics Laboratory ATTN: I. E. Vas Tech. Library Princeton, New Jersey 08540
1	Cornell University Graduate School of Aero Engr ATTN: Library Ithaca, New York 14850	1	Southwest Research Institute Applied Mechanics Reviews 8500 Culebra Road San Antonio, Texas 78228
1	Illinois Institute of Tech. ATTN: M. V. Morkovin 3300 South Federal Chicago, Illinois 60616	1	University of California - San Diego Department of Aerospace and Mechanical Engr Sciences ATTN: Tech. Library La Jolla, California 92037

DISTRIBUTION LIST

No. of Copies	Organization	No. of Copies	Organization

1	University of Colorado
	Department of Astro-Geophysics
	ATTN: E. R. Benton
	Boulder, CO 80302
		1	University of Virginia
			Department of Aerospace
			  Engineering and Engineering
			  Physics
			ATTN: Tech Lib
			Charlottesville, VA 22904

2	University of Maryland
	ATTN: W. Melnik
	        Tech Lib
	College Park, MD 20740
		1	University of Washington
			Department of Mechanical
			  Engineering
			ATTN: Tech Lib
			Seattle, WA 98195

1	University of Michigan
	Department of Aeronautical
	  Engineering
	ATTN: Tech Lib
	East Engineering Building
	Ann Arbor, MI 48104
		1	Virginia Polytechnic Institute
			Department of Aerospace
			  Engineering
			ATTN: G. R. Inger
			Blacksburg, VA 24061

1	University of Santa Clara Department of Physics ATTN: R. Greeley Santa Clara, CA 95053		Aberdeen Proving Ground
1	University of Texas Department of Aerospace Engineering ATTN: J. C. Westkaemper Austin, TX 78712		Marine Corps Ln Ofc Dir, USAMSAA

59